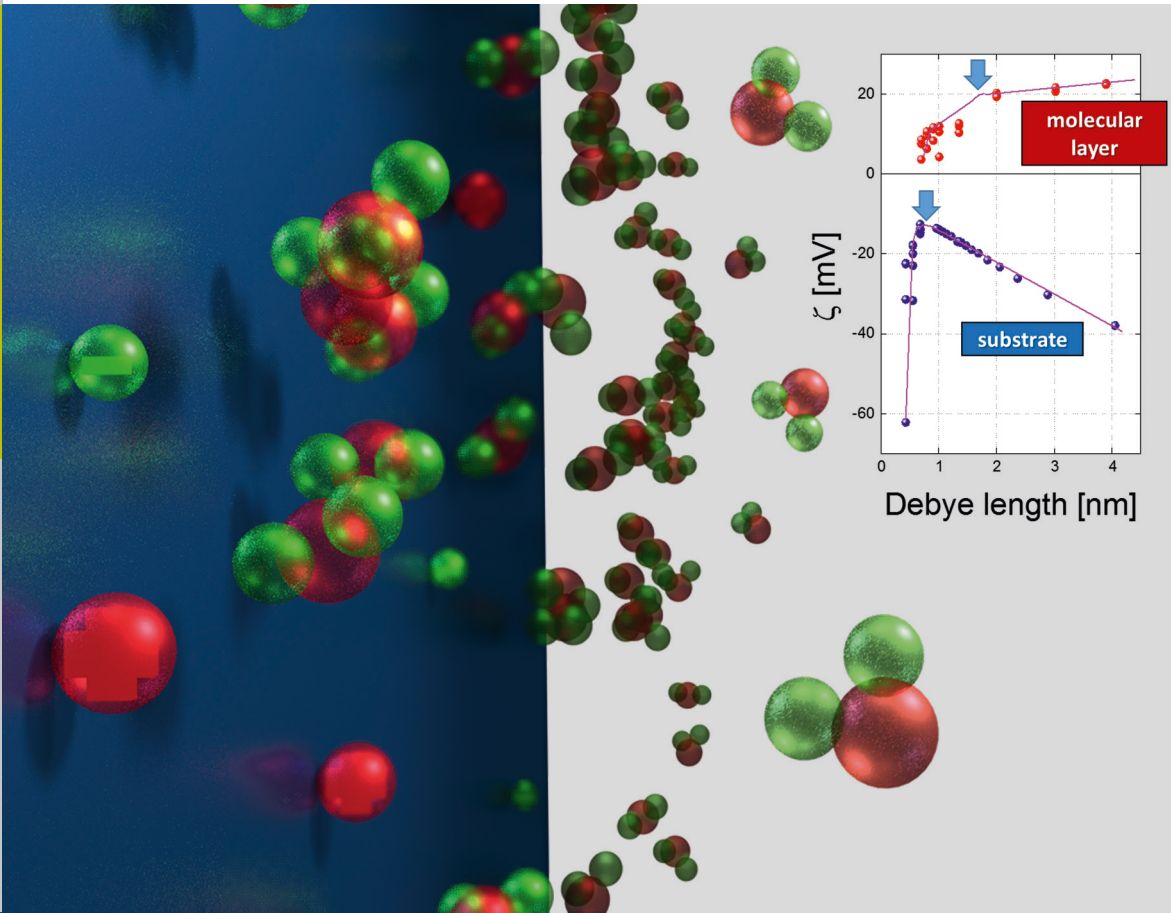


# Surface Potential of Metallic Surfaces and Self-Assembling Organic Monolayers in Various Electrolytes

Junmiao Wang



Schlüsseltechnologien /  
Key Technologies  
Band / Volume 137  
ISBN 978-3-95806-188-0





Forschungszentrum Jülich GmbH  
Peter Grünberg Institute / Institute of Complex Systems  
Bioelectronics (PGI-8 / ICS-8)

# Surface Potential of Metallic Surfaces and Self-Assembling Organic Monolayers in Various Electrolytes

Junmiao Wang

Schriften des Forschungszentrums Jülich  
Reihe Schlüsseltechnologien / Key Technologies

Band / Volume 137

---

ISSN 1866-1807

ISBN 978-3-95806-188-0

Bibliographic information published by the Deutsche Nationalbibliothek.  
The Deutsche Nationalbibliothek lists this publication in the Deutsche  
Nationalbibliografie; detailed bibliographic data are available in the  
Internet at <http://dnb.d-nb.de>.

Publisher and  
Distributor: Forschungszentrum Jülich GmbH  
Zentralbibliothek  
52425 Jülich  
Tel: +49 2461 61-5368  
Fax: +49 2461 61-6103  
Email: [zb-publikation@fz-juelich.de](mailto:zb-publikation@fz-juelich.de)  
[www.fz-juelich.de/zb](http://www.fz-juelich.de/zb)

Cover Design: Grafische Medien, Forschungszentrum Jülich GmbH

Printer: Grafische Medien, Forschungszentrum Jülich GmbH

Copyright: Forschungszentrum Jülich 2016

Schriften des Forschungszentrums Jülich  
Reihe Schlüsseltechnologien / Key Technologies, Band / Volume 137

Master (RWTH Aachen University, 2016)

ISSN 1866-1807  
ISBN 978-3-95806-188-0

The complete volume is freely available on the Internet on the Jülicher Open Access Server (JuSER)  
at [www.fz-juelich.de/zb/openaccess](http://www.fz-juelich.de/zb/openaccess).



This is an Open Access publication distributed under the terms of the [Creative Commons Attribution License 4.0](https://creativecommons.org/licenses/by/4.0/),  
which permits unrestricted use, distribution, and reproduction in any medium, provided the original work is properly cited.

---

## Content

1	Abstract .....	1
2	Introduction.....	2
3	State of the Art and Technology .....	4
3.1	Electrical Double Layer.....	4
3.2	Methods to Determine the $\zeta$ Potential.....	6
3.3	Literature Review.....	8
4	Experimental Implementation .....	11
4.1	Samples and Cleaning Procedures .....	11
4.2	Streaming Potential and Streaming Current Methods .....	13
4.2.1	Electrolytes .....	13
4.2.2	Experiment Setup .....	14
4.2.3	Principle of the Measurement .....	17
5	Results and Discussion .....	20
5.1	Measurements on Polypropylene and Borosilicate Glass.....	20
5.1.1	Polypropylene .....	20
5.1.2	Borosilicate Glass .....	25
5.2	Metallic Surfaces in Chloride Electrolytes.....	26
5.2.1	Oxygen Activated Pt and Au Surfaces in NaCl .....	27
5.2.2	Comparison of Different Chloride Electrolytes .....	29
5.3	Impact of the Electrolyte Concentration on the $\zeta$ Potential .....	30
5.3.1	Basic Consideration .....	31
5.3.2	Reference Measurements on Polypropylene and Borosilicate Glass.....	33
5.3.3	Conductive Surfaces at Higher Electrolyte Concentration .....	36

---

5.3.3.1	Extended EDL Model.....	36
5.3.3.2	$\zeta$ Potential of Pt Thin Films.....	42
5.4	$\zeta$ Potential of Organic Molecules.....	48
6	Conclusions.....	53
7	References.....	55

## 1 Abstract

The aim of this thesis is to systematically investigate the  $\zeta$  potential of different surfaces (polypropylene, borosilicate glass, Pt and Au thin films, and self-assembling monolayer) in different chloride electrolytes XCl (X = Li, Na, or K), focusing on the pH- and concentration-dependent  $\zeta$  potential and the surface treatment with oxygen. The experiments were performed with a modified “SurPASS Electrokinetic Analyzer” using the streaming potential and streaming current methods.

The pH-dependent  $\zeta$  potential analysis of borosilicate glass, Pt, and Au shows that, Pt possesses the highest  $\zeta$  potential, followed by borosilicate glass and Au for all chloride electrolytes. The impact of the different electrolytes on the  $\zeta$  potential is more complex. The oxygen activation of the metallic surfaces seems to lead to the formation of a thin oxide layer, which seems to be less stable for Pt than for Au, whereas we obtained a stable oxygen activation for the oxide borosilicate glass.

At large Debye length (i.e. low electrolyte concentration), the  $\zeta$  potential changes linearly with decreasing Debye length down to a “critical” Debye length. The “critical” Debye length is different for the different surfaces: 0.7 – 0.9 nm for borosilicate glass, 0.5 – 1.2 nm for Pt, and 1.35 – 2 nm for APTES. Below the “critical” Debye length, the  $\zeta$  potential drops strongly. We explain the unusual and transient streaming current-pressure correlation in this regime by a complex adsorption/desorption process for the ions at the surface. As a result, the classic electrical double layer model has to be modified for high electrolyte concentrations. For organic layers this is even more complex, since several surface contributions arising from the molecules and the carrier have to be taken into account.

## 2 Introduction

Generally, deposition processes represent the backbone of many nowadays technologies. These include the deposition of inorganic and organic films as well as the immobilization of biological objects in case of bioelectronic devices.

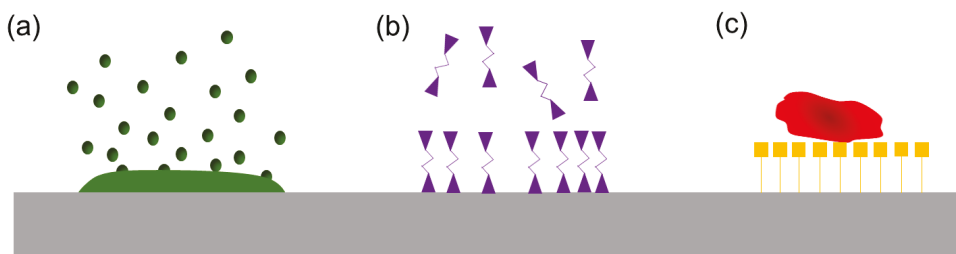


**Figure 2.1:** Sketch of the deposition of inorganic films (a), formation of self-assembling monolayers of organic molecules (b), and biomaterial adhesion (c).

These three typical deposition processes are sketched in Figure 2.1. The thin film deposition describes a technology of growing a very thin film of inorganic or organic material onto a substrate. For the deposition of inorganic films, e.g. metallic layers or oxide films, an oriented growth is often advantageous, even an epitaxial growth is necessary to obtain optimized electronic properties of the layers. Also in case of organic molecules deposition, an ordered adsorption of molecular assemblies to the substrate forming a self-assembling monolayer can be necessary in order to achieve desired results. In case of biological application, it is even more important to modify the substrate in order to enable the immobilization of the biomaterial.

Obviously, the surface properties are crucial in all these deposition processes. Therefore, it is often necessary to tailor the substrate surfaces for the deposition process. One important aspect is the surface potential, which is one of the key interfacial electrokinetic properties. On the one hand, the surface potential strongly depends on the surface conditions, for instance surface activation treatment or termination with special functional groups. On the other hand, the solution used for the deposition process also has an important impact on the surface potential, and, thus, the deposition process. Typically, the

components, pH value, and concentration of the solution are of importance in case of the deposition process at the solid-liquid interface.

In this work, we focus on the surface potential determination of metallic surfaces (noble metals) and self-assembling monolayers of organic molecules in different electrolytes using the streaming potential and streaming current methods. Chapter 3 gives a basic introduction to the surface potential theory and a short state of the art, while chapter 4 describes the experiment details and procedures. In chapter 5 we first investigate the effects of the pH value and different electrolytes on the surface potential at low electrolyte concentration. The oxygen activation treatment of sample surfaces is also discussed. After those, the surface potential of samples is determined in a high electrolyte concentration range of 1 to 1200 mM. Finally, the conclusions are given in chapter 6.

### 3 State of the Art and Technology

Electrokinetic phenomena are a family of effects that describe a liquid moving tangentially to a charged surface. Classic electrokinetic phenomena are electrophoresis, electro-osmosis, streaming potential, and sedimentation potential. In this chapter, first a basic introduction to the electrical phenomenon at the solid-liquid interface is given in section 3.1. In section 3.2 we first sketch the electrokinetic phenomena and then concentrate on the streaming potential and streaming current phenomena. Section 3.3 gives a short literature review of the  $\zeta$  potential measurements with the streaming potential and streaming current methods.

#### 3.1 Electrical Double Layer

Generally, solid surfaces in contact with a polar medium show definite surface charges caused by ionization, ionic adsorption, and ionic dissolution at the interface. These charges influence the neighboring ions in the polar medium. The rearrangement of the charges at the solid surface and the balancing charges in the medium is usually described by the electrical double layer (EDL) model.

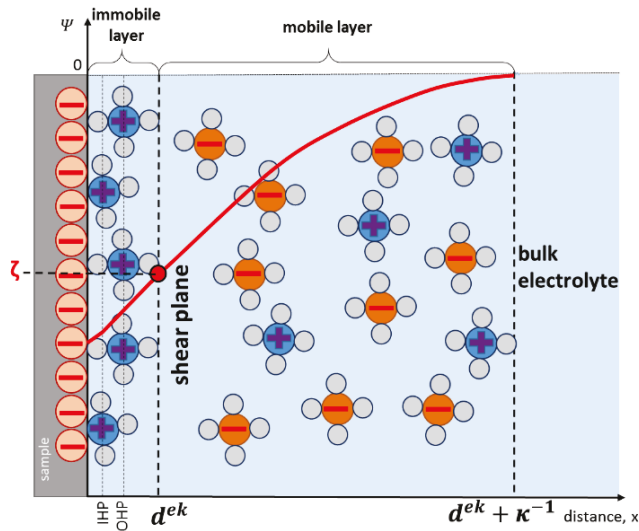


**Figure 3.1:** Schematic structure of the electrical double layer (EDL) according to the Gouy-Chapman-Stern-Grahame (GCSG) theory.

After Georg Quincke first proposed the idea of EDL in 1860, many scientists and researchers have contributed to this issue. Finally, the Gouy-Chapman-Stern-Grahame (GCSG) theory completed the EDL model (see Figure 3.1).

In contact with a polar medium (e.g. liquid electrolyte), solid surface generates charges (for instance negative charges as shown in Figure 3.1). These surface charges influence the distribution of the neighboring ions in the polar medium due to the electrostatic interaction. Ions of the opposite sign are attracted to the surface, and ions of the same sign are repelled. The resulting region, where the ion distribution is different from that in the bulk electrolyte, is called the electrical double layer (EDL). It consists of an immobile layer and a mobile layer (see Figure 3.1). The redistribution of ions in the EDL generates the electrical potential (red line in Figure 3.1) near the charged surface.

In case of Figure 3.1 the negative charges of the surface are partially compensated by the adsorption of the positive charges. Next to the surface, positive ions are strongly attracted to the solid surface and immobilized, forming the immobile layer. The immobile layer can be further divided into the Inner Helmholtz Plane (IHP) defined by the centers of the specifically adsorbed ions and the Outer Helmholtz Plane (OHP) defined by the centers of completely hydrated ions at the distance of their closest approach to the surface. The thickness of the immobile layer is  $d^{ek}$  and normally smaller than 1 nm. Moving from the immobile layer to the bulk electrolyte, the concentration of positive ions gradually reduces to that of the neutral bulk electrolyte. Ions in this region are less affected by the electrostatic interaction and mobile. This layer is called the mobile layer. The thickness of the mobile layer is characterized by the Debye length  $\kappa^{-1}$ . Depending on the bulk ionic strength and the electrical properties of the electrolyte, the Debye length ranges from a few nanometers for high ionic strength electrolytes up to several micrometers for distilled water. The boundary between the immobile layer and the mobile layer is called the shear plane. The electrical potential at the solid surface is difficult to measure directly. However, the electrical potential at the shear plane, called  $\zeta$  potential, can be measured and therefore represents a very important property of the solid-liquid interface.

In conclusion, the  $\zeta$  potential is widely used to characterize the interface between the solid surface and the electrolyte. It is defined by the potential at the shear plane:

$$\zeta = \Psi(d^{ek}) . \quad (3.1)$$

In the immobile layer the potential changes linearly with the distance  $x$ , whereas in the mobile layer it varies exponentially with  $x$ :

$$\Psi(x) = \Psi(d^{ek})e^{-\kappa(x-d^{ek})} . \quad (3.2)$$

Additionally, another important characteristic value – the so-called isoelectric point (IEP) – is widely used. The IEP is defined by the pH value where the  $\zeta$  potential is zero, namely an equilibrium state between negatively and positively charged surface groups. At the isoelectric point, the  $\zeta$  potential is identical to the surface potential (i.e. both are zero). The IEP is a strong indicator for the chemistry of the functional groups that are present on the solid surfaces. This is also where the behavior of surface changes from hydrophilic to hydrophobic.

### 3.2 Methods to Determine the $\zeta$ Potential

Generally, the form of the solid-liquid interface determines the choice of the electrokinetic techniques (see Figure 3.2) for the analysis of the  $\zeta$  potential.

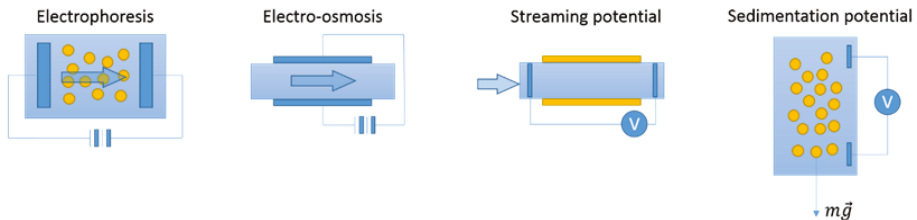


**Figure 3.2:** Sketch of the different classic electrokinetic methods for the analysis of the surface potential ( $\zeta$  potential): (a) particles move in an electrical field, (b) a liquid moves in an electrical field, (c) the pressure gradient causes an electrical potential, and (d) the movement of the particles under the gravitation causes an electrical potential.

Generally, *electrophoresis* appears when charged particles are exposed to an electrical field. Single dispersed particles are electrically charged in the dispersion medium and an

EDL is formed around each of them. The velocity of the particles with respect to a medium at rest is proportional to the  $\zeta$  potential.

*Electro-osmosis* represents the measurement of a liquid flow in a known electrical field. The speed of this flow is proportional to the interaction of the electrical field with the charges of the liquid.

*The streaming potential* arises at a charged surface when a hydrodynamic flow is adjacent to the surface.

*The sedimentation potential* is generated during the movement of electrified particles in gravitational or sedimentation fields in centrifuges.

While electrophoresis and sedimentation potential measurements are dealing with single particle diluted in a colloidal system, electro-osmosis and streaming potential techniques are usually used for particles moving in a defined volume. For the surface potential measurements of surfaces of simple geometry, the streaming potential and electro-osmosis techniques are the best choices.

In this work, the streaming potential method is chosen for the determination of the  $\zeta$  potential. Let us consider a microchannel formed by two parallel planar sample surfaces with channel height  $h$ , width  $W$ , cross section  $A = h \times W$ , and length  $L$  (Figure 3.3).

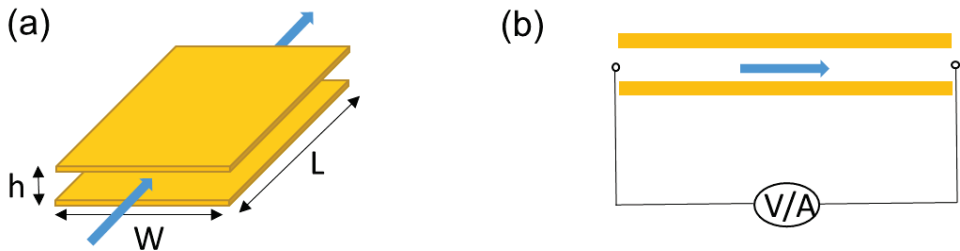


**Figure 3.3:** Parallel plate microchannel (a) for the streaming potential ( $V$ ) and streaming current ( $A$ ) measurements and sketch of the measurement principle (b). The blue arrows indicate the flow direction.

When an electrolyte is forced to flow through the microchannel under an applied hydrostatic pressure  $\Delta p$  between the two ends of the microchannel, the counter ions in

the mobile layer of the EDL are carried downstream resulting in an electric current in the pressure-driven flow direction. This current is known as the streaming current  $I_s$ :

$$I_s = -\frac{\varepsilon\varepsilon_0\zeta A}{\eta L}\Delta p \quad , \quad (3.3)$$

here  $\varepsilon$  is the dielectric constant of the electrolyte,  $\varepsilon_0$  is the vacuum permittivity, and  $\eta$  is the viscosity of the electrolyte. The streaming current can be recorded by the measuring electrodes at the ends of the microchannel, which are connected via a small external resistance (short circuit). If the resistance in the circuit is very large (open circuit), ions accumulate downstream and result in a potential known as the streaming potential  $U_s$ . This streaming potential forces the ions in the mobile layer to move in the direction opposite to the streaming current, thus, generating a current opposite to the streaming current. This current is called the conduction current  $I_c$ :

$$I_c = K_B \frac{A}{L} U_s \quad , \quad (3.4)$$

here  $K_B$  is the total conductivity of the flow microchannel. The streaming potential is then given by  $I_s + I_c = 0$ :

$$U_s = \frac{\varepsilon\varepsilon_0\zeta}{\eta K_B} \Delta p \quad . \quad (3.5)$$

Based on the dependence of the  $\zeta$  potential on the streaming current or streaming potential (equation 3.3 or 3.5), the determination of the  $\zeta$  potential can be achieved by the measurement of the streaming current or the streaming potential.

### 3.3 Literature Review

The  $\zeta$  potential is one of the key interfacial electrokinetic properties to a huge number of natural phenomena, such as electrode kinetics, corrosion phenomena, adsorption processes, crystal growth, colloid stability, and flow characteristics of colloidal suspensions and electrolyte solutions through porous media and microchannels. For macroscopic surfaces of simple geometry (capillaries, channels, planar substrates) at the solid-liquid interface, different electrokinetic techniques, for instance electro-osmosis technique [1] and the streaming potential measurement, can be chosen to measure the  $\zeta$  potential. This work focuses on the latter. Generally, the most important parameters influencing the  $\zeta$  potential of surfaces in an electrolyte are the pH value and the ionic strength of the electrolyte, the electrolyte components, as well as the surface treatment.

We will restrict this review to the following topics: the pH value, the ionic strength, and the components of the electrolyte, and the surface conductance.

The pH-dependent  $\zeta$  potential is of wide interest for researchers. For example, C. Kaulen et al. [2] adjusted the pH value in order to achieve a preferential adsorption of gold nanoparticles on different metals for the fabrication of nanoelectronic devices. In other case it is necessary to investigate the IEP of materials [3] in order to examine the chemistry of the surface functional groups, or the change from hydrophilic to hydrophobic behavior or vice versa.

The effect of the ionic strength of the electrolyte on the  $\zeta$  potential might also be important in order to modify the surface adhesion for certain demands. Based on experimental data at low and medium electrolyte concentration (up to 200 mM), A. Shukla et al. [4] detected a simple and linear correlation between the  $\zeta$  potential and the Debye length. Meanwhile, one application report of Anton Paar [5] stated a similar correlation between the  $\zeta$  potential and the ionic strength, and extrapolated the  $\zeta$  potential to high ionic strength. They demonstrated a finite  $\zeta$  potential at high ionic strength (1 M). Later we will show that this extrapolation is questionable. However, most of the streaming potential measurements of the  $\zeta$  potential [2, 6-7] are performed at low electrolyte concentration (0.001 – 10 mM), and only a few experiments [4-5] are extended to relatively higher concentration (200 mM).

In a salt electrolyte, preferential adsorption of ions on the membrane surfaces and, thus, their effect on the  $\zeta$  potential can be crucial for certain special demands. S. Salgin et al. [7] analyzed the effect of various chloride and potassium salts on the  $\zeta$  potential in the concentration range of 0.001 – 0.1 M. E. E. Saka et al. [8] demonstrated that at any monovalent electrolyte concentration, the magnitude of the  $\zeta$  potential increases with the electrolytes in the order  $\text{Li}^+$ ,  $\text{Na}^+$ ,  $\text{K}^+$ ,  $\text{Rb}^+$ , to  $\text{Cs}^+$  due to the hydration degree of the ions.

In addition to the  $\zeta$  potential, another important interfacial electrokinetic parameter is the surface conductance. The surface conductance usually refers to the electronic conductance of the substrate or a thin layer at the surface of the substrate, where a net charge can accumulate due to the charging of the solid-liquid interface. As for non-conductive surfaces or surfaces with small conductance, the  $\zeta$  potential can be easily determined with the streaming potential method by using the corresponding Helmholtz-

Smoluchowski equations. D. Erickson et al. [6] improved the classic “slope–intercept method” by adding two correction parameters to determine the  $\zeta$  potential and surface conductance at different channel heights. C. Werner et al. [9] analyzed the impact of the surface conductance on the total conductance of the measuring cell and performed standard streaming potential measurements. However, for samples with conductive membranes, the contribution of the membrane body to the total conductance of the membrane-channel-membrane system must be taken into account, since the streaming current and the conduction current involved in this case do not flow through the identical path, i.e. the streaming current flows only through the slit channel formed by the two membrane samples facing each other, whereas a non-negligible part of the conduction current is likely to flow through the membrane pores filled with electrolyte solution [10-14]. As a result, the  $\zeta$  potential determined by the streaming potential method and the streaming current differ strongly. In this case the streaming current method is a better choice to determine the  $\zeta$  potential. A. M. Gallardo-Moreno et al. [11] compared these two methods and demonstrated that for conductive surfaces (e.g. metals), the contribution of conductivity of the sample to the cell resistance leads to unrealistic values. P. Fievet et al. [10] and H. Xie et al. [12] demonstrated that the measured streaming current can be extrapolated to a membrane thickness of zero to determine the real  $\zeta$  potential of each component.

## 4 Experimental Implementation

In this chapter, the sample preparation and cleaning procedures are introduced. Furthermore, the principle of the  $\zeta$  potential measurement, namely the streaming potential and streaming current methods, is discussed.

### 4.1 Samples and Cleaning Procedures

In this work, the surface potential characterization is investigated for different surfaces:

- i. Polypropylene foil (PP) is used for the calibration of the system and also as reference measurements, since it can withstand many chemicals that are usually used during the experiments and provide reproducible results.
- ii. Borosilicate glass (BSG) consists of silicon dioxide (> 80%), boron oxide (> 10%), and other minor oxides (~10%), and has an inert and hydrophilic surface. It is used as substrate for all the metallic thin films and organic layers.
- iii. Two types of metallic surfaces are chosen, namely evaporated platinum (Pt) thin films and sputtered gold (Au) thin films on borosilicate glass. The typical thickness of these thin films is 5 – 10 nm.
- iv. Self-assembling monolayers (SAMs) of 3-aminopropyltriethoxysilane (APTES) are also characterized. SAMs are ordered molecular assemblies that are formed spontaneously by the adsorption to the substrate. The molecule (Figure 4.1a) consists of a head group, which is chemisorbed to a specific substrate, a molecular backbone, and an end (functional) group, which can possess different functionalities.

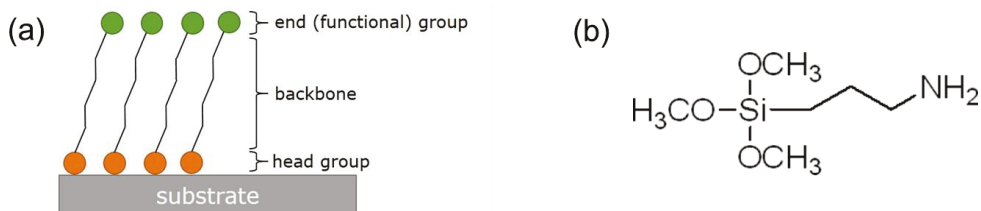


**Figure 4.1:** Schematic structure of SAMs (a) [15] and the structure of APTES (b).

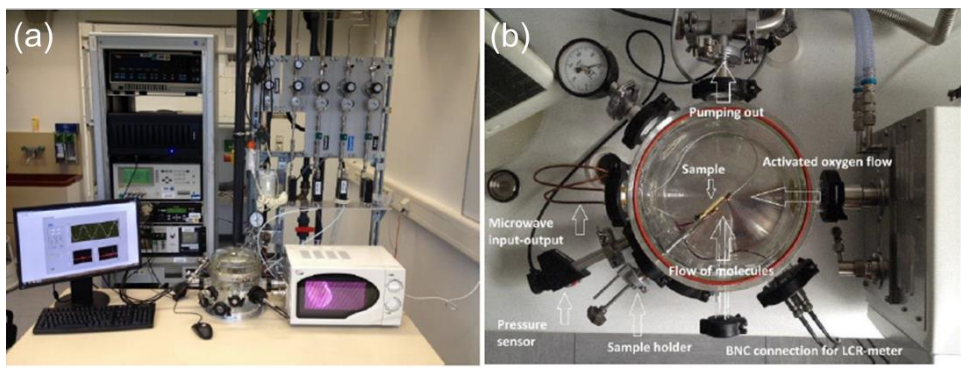


**Figure 4.2:** GLOBUS – a novel concept for the deposition of molecular monolayers, including in-situ cleaning and activation of substrates as well as in-situ electronic characterization of molecular monolayers: (a) overview, (b) top view of the deposition chamber.

APTES (Figure 4.1b) with amino as functional group is deposited on BSG using our constructed device “GLOBUS” shown in Figure 4.2. The deposition of APTES is as follows [16]. Chemically cleaned BSG substrates are placed on a sample holder in the recipient of GLOBUS. A beaker with an APTES molecule source is connected to the deposition chamber. The recipient is evacuated. Using a flow of oxygen through the microwave, ozone is generated and directed to the substrates. The ozone will remove organic residuals and activate the surfaces. After activation, the recipient is set to a constant pressure of nitrogen, typically approximately 1 mbar for APTES deposition. Then the valve connecting APTES source with the recipient is opened. APTES molecules evaporate, enter the chamber, and some of them deposit onto the BSG. After some time the valve is closed. Additional molecules are removed by constant nitrogen pumping to obtain a SAM of APTES. The typical thickness of the monolayer of APTES is about 0.7 nm.

Since our work focuses on the surface potential of different samples, the cleaning of the sample surface and the measuring system is a very important part of the preparation. This is especially important, since the streaming potential and streaming current methods are extremely sensitive to any contamination at the surface.

Before measurements, samples undergo a chemical cleaning procedure:

- i. Chemically cleaning in acetone for 5 minutes in an ultrasonic bath at 25 °C with 100% power (320 W) at 80 kHz frequency, then
- ii. chemically cleaning in propanol for 5 minutes in an ultrasonic bath at 25 °C with 100% power (320 W) at 80 kHz frequency, then
- iii. drying samples with nitrogen.

Oxygen activation treatment is used to remove the organic contamination at the surface. At the same time it leads to the surface activation for BSG and even an oxidation for the metallic films. The oxygen activation surface treatment is performed also in the GLOBUS (see Figure 4.2). Samples are placed in the deposition chamber that is then evacuated. After applying a pure oxygen flow, oxygen plasma is generated in a glass chamber inside a microwave oven. The samples are activated by the ozone flow from the microwave oven at 1 mbar for 3 minutes.

As for the cleaning of the SurPASS measuring system, the system is rinsed with 2 L MilliQ water after every complete series of measurements. The electrolyte beaker is usually cooked with MilliQ water at about 80 °C for several times.

## **4.2 Streaming Potential and Streaming Current Methods**

The streaming potential and streaming current methods represent the best suitable technique for the surface potential investigation of planar samples in an electrolyte. In our work, these methods are applied by using a modified “SurPASS Electrokinetic Analyzer” (Anton Paar GmbH).

### **4.2.1 Electrolytes**

In this work, different electrolytes are used and they are divided into two groups: working electrolyte and titration electrolyte including acidic titration electrolyte and basic titration electrolyte (see Table 4.1). The solvent is the double demineralized water or MilliQ water (at 25 °C, resistivity: 18.2 MΩ·cm, Total Organic Carbon < 5 ppb).

**Table 4.1:** Different electrolytes used in the experiments

working electrolyte	acidic titration electrolyte	basic titration electrolyte
NaNO <sub>3</sub>	HNO <sub>3</sub> (50 mM)	NaOH (10 mM)
KCl	HCl (50 mM)	KOH (10 mM)
NaCl	HCl (50 mM)	NaOH (10 mM)
LiCl	HCl (50 mM)	LiOH (10 mM)

#### 4.2.2 Experiment Setup

The streaming potential and streaming current measurements are performed using a modified “SurPASS Electrokinetic Analyzer” (see Figure 4.4).

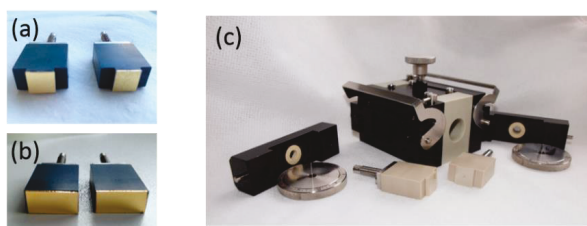


**Figure 4.3:** The samples are attached to the sample holders (a) or (b) and then placed into the measuring cell (c) to form the microchannel [15].

For the measurements, a pair of identical samples (10 × 10 or 20 × 10 mm) is attached to the sample holders (Figure 4.3a or b) using double-sided adhesive tape. These two sample holders are mounted inside the measuring cell (Figure 4.3c) to form a microchannel. It is recommended that the distance between the planar surfaces (gap height) is adjusted to approximately 100 μm in order to form a laminar flow.

Next to SurPASS is a reservoir with the working electrolyte beaker (see Figure 4.4). The properties of the electrolyte are controlled via a temperature sensor, a conductivity sensor, and a pH sensor. During the measurements, all parameters (i.e. voltage or current, pressure gradient, cell resistance, and the temperature, conductivity and pH value of the electrolyte) are recorded or controlled by the software (VisioLab).

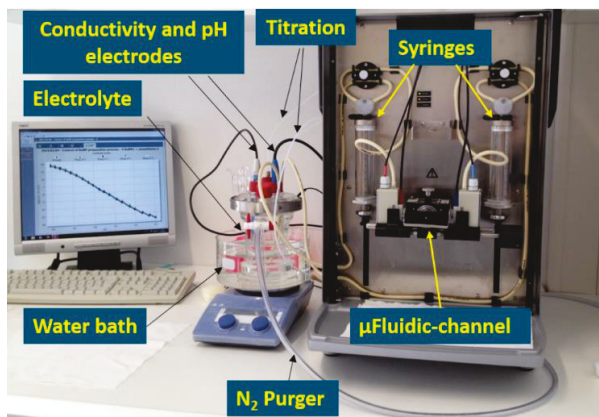


**Figure 4.4:** Overview of the streaming potential and streaming current setup (SurPASS electrokinetic analyzer) [15].

The measurement setup was optimized with two major modifications. The first is the introduction of a water bath with a constant temperature and a magnetic stir bar for the electrolyte (see Figure 4.4). This allows the stabilization of the temperature of the electrolyte. This is important since the  $\zeta$  potential depends on the viscosity and dielectric constant of the electrolyte, which are temperature dependent. The second important modification is the continuous purging of the working electrolyte with  $N_2$  (see Figure 4.4 and 4.5). The purpose of this purger is to reduce or eliminate the dissolved  $CO_2$  in the electrolyte, which can cause unpredictable behavior [17]. Nitrogen was chosen because of its availability and relatively lower price.

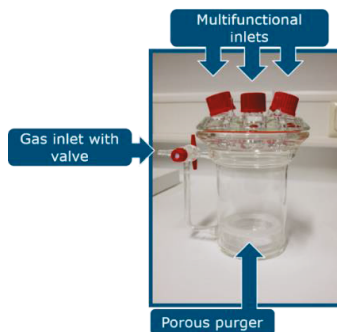


**Figure 4.5:** Electrolyte beaker with inlets for the sensors and  $N_2$  purger [15].

In order to provide reproducible and reliable results, it is necessary to calibrate the pH sensor and the conductivity sensor before a long series of experiments or at least once a month. The calibration results are recorded and analyzed in order to keep the sensors in good conditions. The calibration of the pH sensor requires three standard buffer solutions of known pH values. After the calibration, the characteristics of the pH electrode, i.e. the electrode slope and the offset potential at pH 7 are saved in the SurPASS firmware. The calibration of the conductivity sensor is a single point calibration and requires a standard conductivity solution. After calibration, the cell constant of the conductivity sensor is saved in the SurPASS firmware. The results of sensors calibration are shown in Figure 4.6.

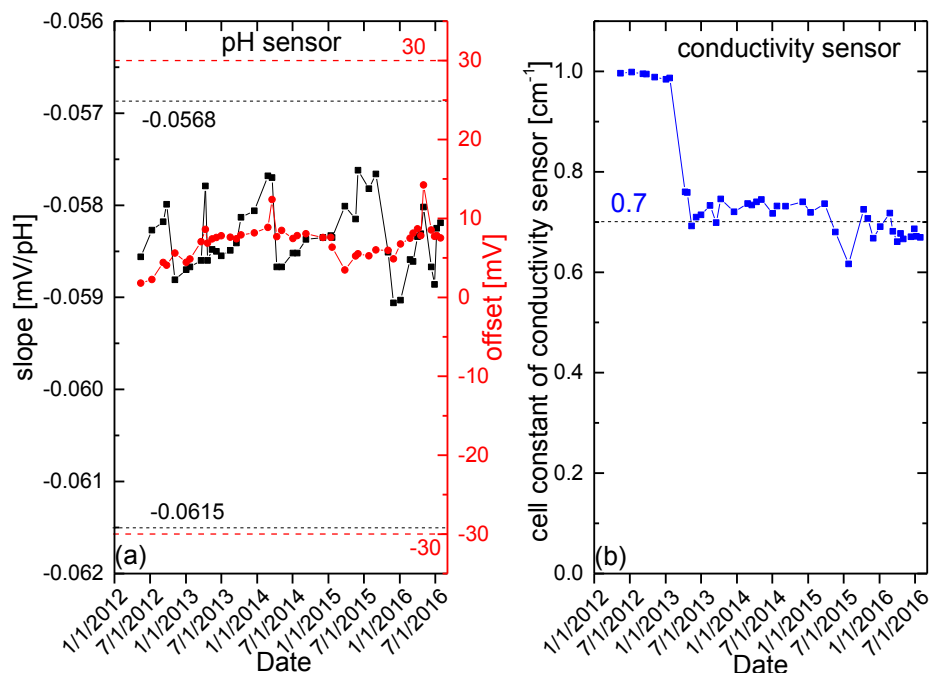


**Figure 4.6:** Calibration results of the pH sensor (a) and the conductivity sensor (b). The dashed lines in (a) indicate the allowed range for calibration.

The pH sensor calibration results show a slope range of -0.0590 to -0.0575 mV/pH and an offset range of 0 to 10 mV at 25 °C, which are in the acceptable ranges (slope: -0.0592 mV/pH  $\pm$  4% and offset:  $\pm$ 30 mV). The conductivity sensor calibration results show a cell

constant about  $0.7 \text{ cm}^{-1}$ . This cell constant of the conductivity sensor is exactly the conductivity sensor calibration factor  $F$ , which will be used in the further measurements. All calibration results in Figure 4.6 indicate that the sensors were kept in good conditions.

### 4.2.3 Principle of the Measurement

The preparation procedures are as follows:

- i. Samples are mounted to the sample holders with double-sided adhesive tape, which are then mounted into the measuring cell.
- ii. Then the measuring cell is connected to the tubes that lead the electrolyte via the syringes to the microchannel formed inside the measuring cell. Each tube contains a pressure sensor and an Ag/AgCl electrode to measure the voltage or current, depending on the electrical circuit.
- iii. The beaker with the fresh working electrolyte is prepared with a magnetic stir bar and nitrogen purger.
- iv. Before the measurement, the system has to be rinsed with 100 ml of fresh working electrolyte and afterwards the electrolyte is poured out to a “waste beaker”.
- v. After the rinsing, the gap height of the measuring cell is adjusted to about  $100 \mu\text{m}$ .
- vi. Then the “flow check” procedure is performed to make sure that the system is filled without air and to check the parallel mounting of samples.

After the preparation, the measurement is performed as follows. The pressure gradient (from 0 to  $\pm 400 \text{ mbar}$ ) is generated via a pair of motorized syringes that move synchronically, pushing the electrolyte through the measuring cell in both directions (ramp 1 and ramp 2). The movement of a liquid through the capillary system creates a streaming potential or streaming current, which, together with the pressure, is recorded by the electrodes and pressure sensors, respectively. These data are then processed by the software (VisioLab) as in Figure 4.7b:

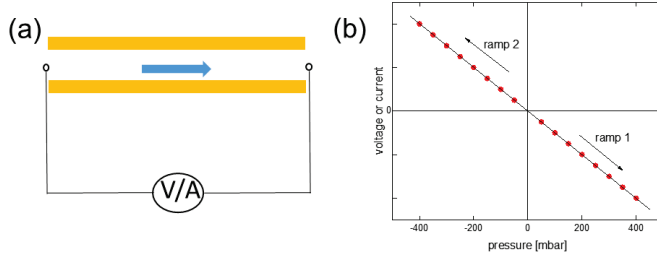


**Figure 4.7:** Sketch of the measurement principle (a) and determination of the  $\zeta$  potential by recording voltage or current as function of the pressure gradient across the microchannel of the measuring cell (b).

The streaming potential and streaming current should linearly depend on the pressure (Figure 4.7b). The slope  $dU/dp$  or  $dI/dp$  is used to determine the  $\zeta$  potential using the Helmholtz-Smoluchowski equation:

$$\zeta = \frac{dU}{dp} \frac{\eta}{\varepsilon \varepsilon_0} \frac{L}{AR} \quad \text{or} \quad (4.1)$$

$$\zeta = \frac{dI}{dp} \frac{\eta}{\varepsilon \varepsilon_0} \frac{L}{A} \quad , \quad (4.2)$$

where  $I$  is the streaming current,  $U$  is the streaming potential,  $p$  is the pressure applied between the ends of the measuring cell,  $\eta$  is the viscosity of the electrolyte,  $\varepsilon_0$  is the vacuum permittivity,  $\varepsilon$  is the dielectric constant of the electrolyte,  $L$  is the length of the microchannel,  $A = W \times h$  is the microchannel cross section, with width  $W$  and gap height  $h$ , and  $R$  is the electrical resistance of the microchannel cell. Parameters  $\eta$  and  $\varepsilon$  are taken from the table in the SurPASS.

In our work, typically two kinds of standard measurements are applied: the stability test and the titration test. A stability test consists of a number of single measurement, during which, the  $\zeta$  potential and all other parameters are recorded without any change of the setting. The streaming current method is chosen for this test and every stability test lasts typically 3 h. The titration test is performed by stepwise adding titration electrolytes into the working electrolyte. Between two titration steps, the  $\zeta$  potential is determined and recorded with all other parameters. The titration electrolyte can be acid, base, or highly

concentrated working electrolyte (see Table 4.1), and the corresponding titration tests are acidic titration test, basic titration test, or concentration test, respectively. In the titration test, the streaming potential method and the streaming current method can be chosen by the user.

Although the measurements are automated to some degree and performed using the conventional electrokinetic analyzer, it is still a challenge to obtain reliable and reproducible results due to many factors ranging from the preparation of the samples to special measurement procedures, which forced us to always pay extreme attention to the measurement process.

## 5 Results and Discussion

In this chapter, the surface potential of different surfaces and its modification for instance via surface activation or concentration variation of the electrolyte are discussed. Starting with simple surfaces (polypropylene) and borosilicate glass as reference measurements, we take a closer look at metallic surfaces of noble metals (Pt and Au) and examine their behavior in different electrolytes. Then we discuss the effect of electrolyte concentration variation on the  $\zeta$  potential. We demonstrate that this not only changes the Debye length, thus, the thickness of the mobile layer of the EDL. At high concentration it also changes the EDL itself and strongly affects the measurements. Finally, we apply our finding to more complex system, i.e. self-assembling monolayers of organic molecules.

### 5.1 Measurements on Polypropylene and Borosilicate Glass

In this section, we first discuss reference measurements on polypropylene (PP) and borosilicate glass (BSG). The latter is used as substrate for all further experiments. We will concentrate on the pH dependence of the  $\zeta$  potential of PP and BSG at different electrolyte concentrations and the isoelectric point (IEP).

#### 5.1.1 Polypropylene

PP is an isotactic polymer with a perfect inert and hydrophobic surface. Since PP can withstand chemicals that are normally used during the experiments and provide reproducible and reliable results, therefore it is used to calibrate the measuring system.

Generally, a test of the stability of the experiment setup is first performed. For 3 h, PP is continuously measured without changing any parameters. After this stability test, PP undergoes a stepwise acidic titration test starting from the neutral pH range. In the experiments, the streaming potential measurement and the streaming current measurement are simultaneously applied. For the acidic titration, sodium nitrate ( $\text{NaNO}_3$ , double demineralized water as solvent) is used as working electrolyte and nitric acid ( $\text{HNO}_3$ , 50 mM) as titration electrolyte, the sample size is  $10 \times 10$  mm. Typical current-pressure correlation and voltage-pressure correlation are shown in Figure 5.1a and b, respectively.

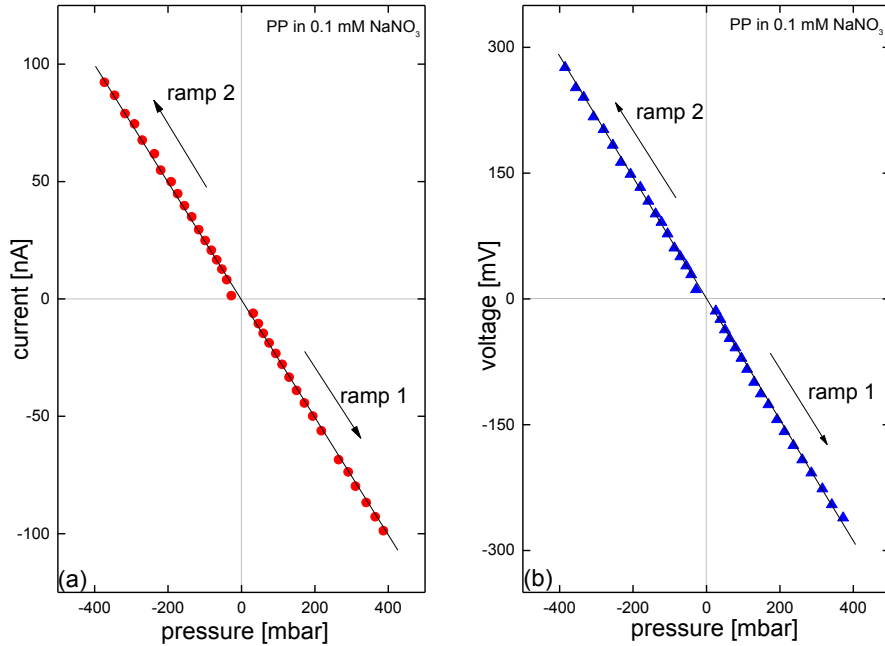


**Figure 5.1:** Streaming current (a) and streaming potential (b) measurements for polypropylene in 0.1 mM NaNO<sub>3</sub>.

Driven by a pressure gradient the electrolyte streams through the microchannel in both directions (first ramp 1 and then ramp 2). From Figure 5.1 it can be seen that the measurements on PP show an excellent linear dependence of current and voltage on the pressure. The linearity correlation factor  $R$  is usually larger than 0.998. The slopes  $dI/dp$  and  $dU/dp$  are used to determine the  $\zeta$  potential using the Helmholtz-Smoluchowski equations:

$$\zeta = \frac{dI}{dp} \frac{\eta}{\epsilon \epsilon_0} \frac{L}{A} \quad \text{and} \quad (5.1)$$

$$\zeta = \frac{dU}{dp} \frac{\eta}{\epsilon \epsilon_0} \frac{L}{AR} \quad , \quad (5.2)$$

where  $I$  is the streaming current,  $U$  is the streaming potential,  $p$  is the pressure applied between the ends of the measuring cell,  $\eta$  is the viscosity of the electrolyte,  $\epsilon_0$  is the vacuum permittivity,  $\epsilon$  is the dielectric constant of the electrolyte,  $L$  is the length of the microchannel,  $A = W \times h$  is the microchannel cross section, with width  $W$  and gap height

$h$ , and  $R$  is the electrical resistance of the microchannel cell. During the experiment,  $dI/dp$  or  $dU/dp$  and the pH value, conductivity and temperature of the electrolyte are recorded. Together with the viscosity  $\eta$ , dielectric constant  $\epsilon$ , and dimensions of the measuring cell, which are known, the  $\zeta$  potential can be evaluated.

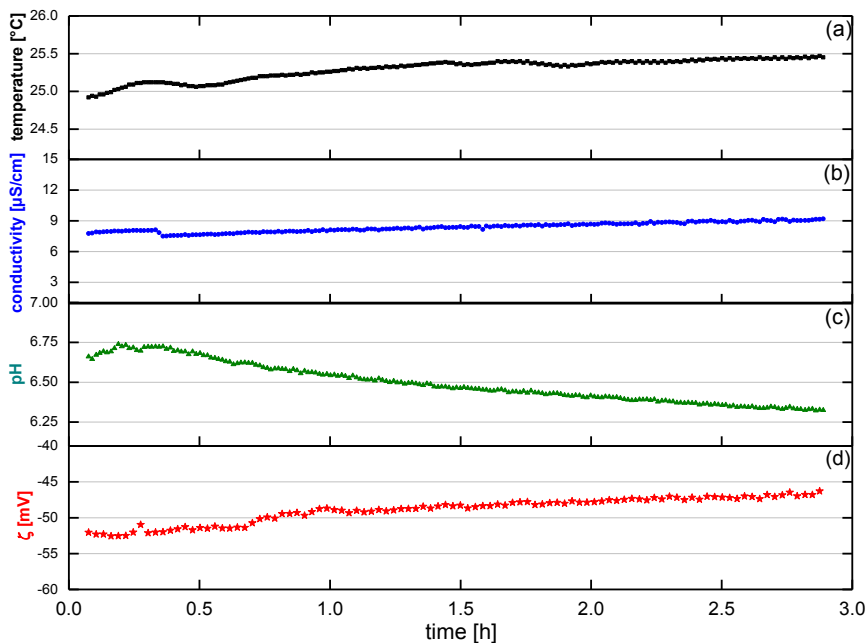


**Figure 5.2:** A stability test for polypropylene in 0.1 mM  $\text{NaNO}_3$  showing the time dependence of the temperature (a), conductivity (b) and pH (c) of the electrolyte together with the  $\zeta$  potential (d).

Figure 5.2 shows a stability test of the system for PP in 0.1 mM  $\text{NaNO}_3$ . In order to obtain such stable reading, experiments are performed with a well-tempered reservoir by using a water bath. The temperature of this water bath is set to 25 °C, which provides a quite stable electrolyte temperature of 25 – 25.5 °C (black symbols). The control of the electrolyte temperature is important, since the viscosity  $\eta$  and dielectric constant  $\epsilon$  of the electrolyte depend on the electrolyte temperature. Within this 3 h stability test, the electrolyte conductivity (blue symbols) is also quite stable. This is among others achieved by using a  $\text{N}_2$  purger for continuous purging of the electrolyte. However, the most

important parameter that has to be stabilized is the pH value of the electrolyte. Here the  $N_2$  purger is also very important. However, we also noticed that a small amount of contaminations leads to modification of the pH in time. These contaminations could come from the cleaning procedures of the electrolyte beaker, or acid or base that remained in the different components. In the example shown in Figure 5.2, the pH value (olive symbols) decreases from 6.75 to 6.33 most likely due to some acid remains in the porous structure of the electrolyte beaker. Since the pH decreases, the  $\zeta$  potential (red symbols) correspondingly increases. Figure 5.2 demonstrates, why it is important to test the stability of the setup prior to each experiment series like a titration run or a concentration series. By performing a proper stability test, all parameters are well monitored and the system is stabilized in order to perform further measurements.

In order to investigate the pH dependence of the  $\zeta$  potential of PP, acidic titration tests for PP in  $NaNO_3$  are done. Since the PP surface is non-conductive, both the streaming potential method and the streaming current method can be applied and should yield identical values for the  $\zeta$  potential. Typical acidic titration tests are shown in Figure 5.3. In the experiments a stability test (small dots) is first performed using the streaming current method. Acidic titration tests are alternatively performed with the streaming potential method (solid triangles) and the streaming current method (open triangles) in 0.1 mM  $NaNO_3$  (black triangles), 1 mM  $NaNO_3$  (red triangles) and 10 mM  $NaNO_3$  (blue triangles).

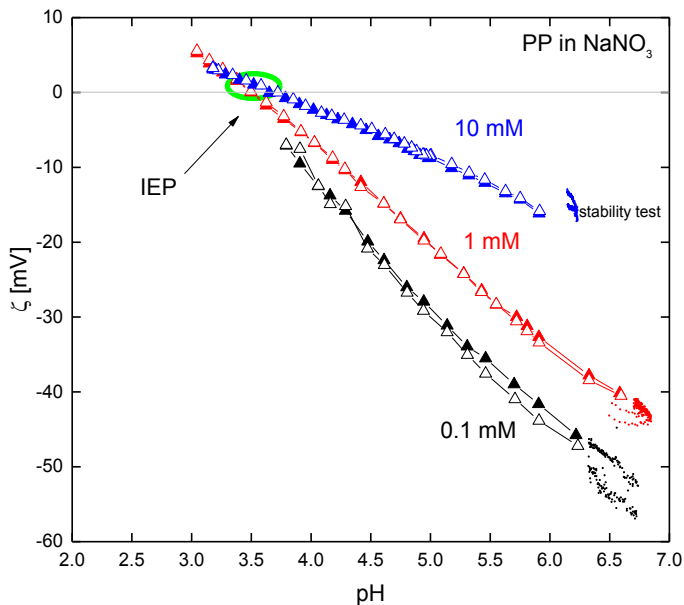


**Figure 5.3:** Stability test (small dots) and pH dependence of the  $\zeta$  potential (large triangles) for PP in NaNO<sub>3</sub> electrolyte with different concentrations for the streaming current measurements (open triangles) and the streaming potential measurements (solid triangles).

In aqueous solution, the charges on inert surfaces are generated only by the adsorption of water ions ( $\text{OH}^-$  or  $\text{H}_3\text{O}^+$ ). This leads to a linear dependence of the  $\zeta$  potential on the pH value, and an isoelectric point (IEP) of pH 4. At the IEP, an equilibrium state of absorbed negative water ions ( $\text{OH}^-$ ) and positive water ions ( $\text{H}_3\text{O}^+$ ) at the surface is reached [18]. According to the literatures [19-22], PP shows a linear dependence of the  $\zeta$  potential on the pH value, and an IEP of  $\text{pH } 3.5 \pm 0.5$ . Our measurements in Figure 5.3 show nearly identical values for the  $\zeta$  potential for the streaming potential method and the streaming current method, a linear dependence of the  $\zeta$  potential on the pH value, and an IEP around pH 3.5 corresponding to the literature values of  $\text{pH } 3.5 \pm 0.5$ . Therefore, measurements demonstrate that the setup works properly.

### 5.1.2 Borosilicate Glass

BSG is one of the most suitable substrates for organic or bioelectronics samples. It consists of silicon dioxide (> 80%), boron oxide (> 10%), other minor oxides (~10%), and has an inert and hydrophilic surface. In this work, BSG is used as the substrate for all the metallic and organic films that are examined later. The characterization of the surface of BSG is therefore used as reference measurements.

In this analysis, standard stability tests followed by acidic titration tests are performed. Here potassium chloride (KCl, MilliQ water as solvent) is used as the working electrolyte and hydrochloric acid (HCl, 50 mM) is the titration electrolyte. The sample size is 10 × 10 mm. BSG samples are first chemically cleaned with acetone and propanol.

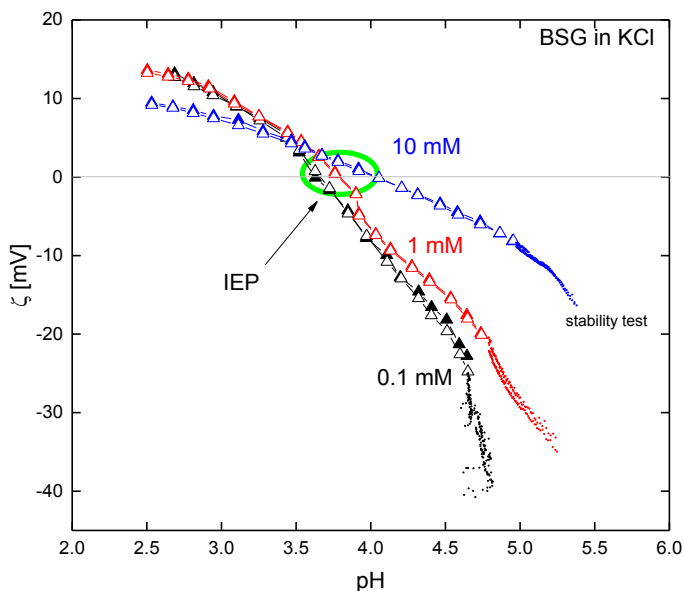


**Figure 5.4:** Stability test (small dots) and pH dependence of  $\zeta$  potential (large triangles) for BSG in KCl electrolyte with different concentrations for the streaming current measurements (open triangles) and the streaming potential measurements (solid triangles).

The pH dependence of the  $\zeta$  potential of BSG is shown in Figure 5.4. The experimental data show that the streaming current and streaming potential measurements yield

identical values for the  $\zeta$  potential, the BSG surface seems to be inert, and the  $\zeta$  potential increases with the increasing KCl concentration, which is also found for PP. However, the IEP seems to increase from pH 3.5 to 4.0 with increasing electrolyte concentration. At first sight, this looks strange. However, also in the literature different IEP values are reported ranging from pH 3.5 [15], 2.8 – 3.2 [23] to even 2 – 4 (silicon surfaces) [24-25]. The slight curvature at low pH value is always present and usually interpreted in terms of overcharging effect, due to the large density of counter-ions in the electrolyte [26].

In this chapter we show:

- i. The measurements on PP and BSG demonstrate the reliability of the optimized setup for the streaming current and streaming potential measurements.
- ii. We demonstrate the necessity of the stability test.
- iii. Furthermore, these measurements can serve as reference for the further experiments.

## 5.2 Metallic Surfaces in Chloride Electrolytes

Metallic surfaces (noble metals) are not only of great interest in conventional electronics, they also play an important role for organic electronics and bioelectronics applications. They are mostly used as electrode materials or substrates for the deposition of organic components or immobilization of biological objects. In these cases, the deposition usually takes place by exposing the metallic surface to a liquid solution, which contains the organic or biological components that should be deposited or immobilized on the metallic surface. In many cases, the pH value of the solution plays an important role for the deposition. Very often the basic regime ranging from pH 6 to 9 is used. In order to understand the deposition process, it is important to know and understand the surface properties of the metallic layer in the electrolyte. In this section, we analyze the pH-dependent  $\zeta$  potential of platinum (Pt) and gold (Au) thin films in detail. Different chloride electrolytes XCl (X = Li, Na, or K) are used and the role of the oxygen activation of the surface is tested.

Pt and Au thin films are deposited via thermal evaporation or sputter deposition on borosilicate glass (BSG). In order to avoid a too large conductivity that hinders the surface

potential measurement, a film thickness of  $\sim 10$  nm is chosen. In order to improve the sensibility of the measurement, a sample size of  $20 \times 10$  mm is chosen. Prior to the  $\zeta$  potential measurement, the sample surfaces are activated with oxygen at 1 mbar for 3 minutes. The working electrolyte is 10 mM XCl ( $X = \text{Li}, \text{Na}, \text{or K}$ ), and the corresponding titration electrolyte is 10 mM XOH ( $X = \text{Li}, \text{Na}, \text{or K}$ ). Since the Pt and Au thin films still have a large surface conduction, only the streaming current method can be used to measure the  $\zeta$  potential.

### 5.2.1 Oxygen Activated Pt and Au Surfaces in NaCl

In order to get a first impression of the different surface properties and the impact of the surface activation, plain BSG substrates and Pt and Au coated BSG are analyzed in NaCl electrolyte (10 mM) directly after oxygen activation. After a first basic titration test (typically from pH 6 to 9), an optional second titration follows. In all cases a final titration test is done approximately 20 hours later. This allows to examine the stability of the oxygen activation, which represents an important factor of the activation.

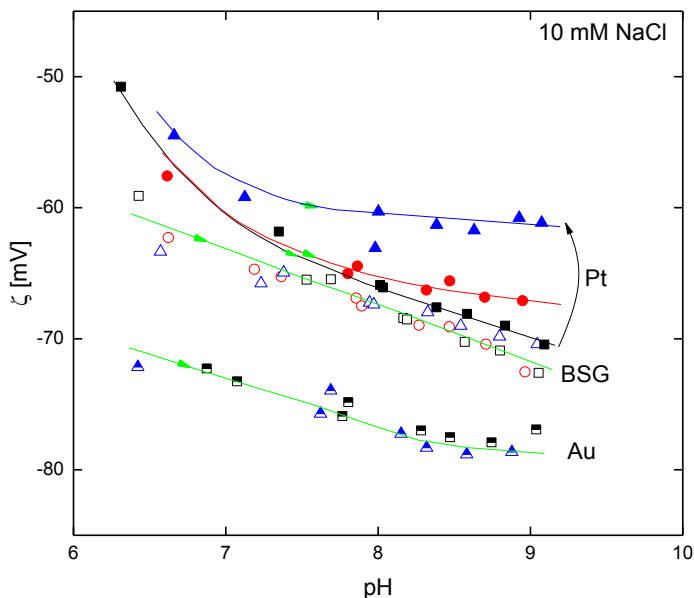


**Figure 5.5:** Time- and pH-dependent  $\zeta$  potential of BSG (open symbols), Pt (10 nm, solid symbols), and Au (10 nm, semi-solid symbols) in 10 mM NaCl.

The time- and pH-dependent  $\zeta$  potential of activated BSG, Pt, and Au thin films are shown in Figure 5.5. Directly after oxygen activation, the samples undergo a first basic titration (squares) and an optional consecutive basic titration (circles), followed by the last basic titration (triangles) approximately 20 h after the oxygen activation. Each titration test lasted about 2.5 h. The lines in Figure 5.5 serve as guide for the eye, and the arrows indicate the direction of titration.

Starting from the neutral pH range, the BSG substrate, Pt and Au thin films undergo stepwise basic titrations from pH 6 to 9. There are mainly three important points in Figure 5.5:

- i. Considering the IEP of the materials that should range between pH 3 and 4 (values of pH 3.4, 3.75, and 3.8 are reported for BSG, Au, and Pt, respectively [15]), the pH-dependence of all surfaces seems to indicate a basic or even amphoteric behavior. However, this is not expected for these systems. It is more likely that the surface potential saturates at high values (positive as well as negative).
- ii. Generally, the highest  $\zeta$  potential is observed for the Pt films, whereas Au films show the lowest (most negative)  $\zeta$  potential.
- iii. Finally, Au and BSG do not show any modification of the surface potential with time. Thus, the activation with oxygen seems to produce a very stable surface state, which is not affected by the exposure to the electrolyte for 1 day. In case of BSG, it is known that the oxygen treatment activates the oxide on the surface. In case of the metallic layers, the oxygen treatment forms an oxide layer [27-28]. For Au, this layer seems to be quite stable, whereas for Pt the oxide layer seems to be less stable. The  $\zeta$  potential increases with time for Pt. The oxygen activation forms an oxide layer on Pt, which is not stable. During the experiment the oxide layer is removed or partially removed, which leads to a significant increase of the  $\zeta$  potential values in the last basic titration (solid triangles).

The results demonstrate that the surface treatment of metallic surfaces plays an important role for the surface properties.

## 5.2.2 Comparison of Different Chloride Electrolytes

In the next step, we will try to compare the impact of different electrolytes on the surface potential of the metallic films. For this we chose chloride electrolyte XCl with X = Li, Na, and K.

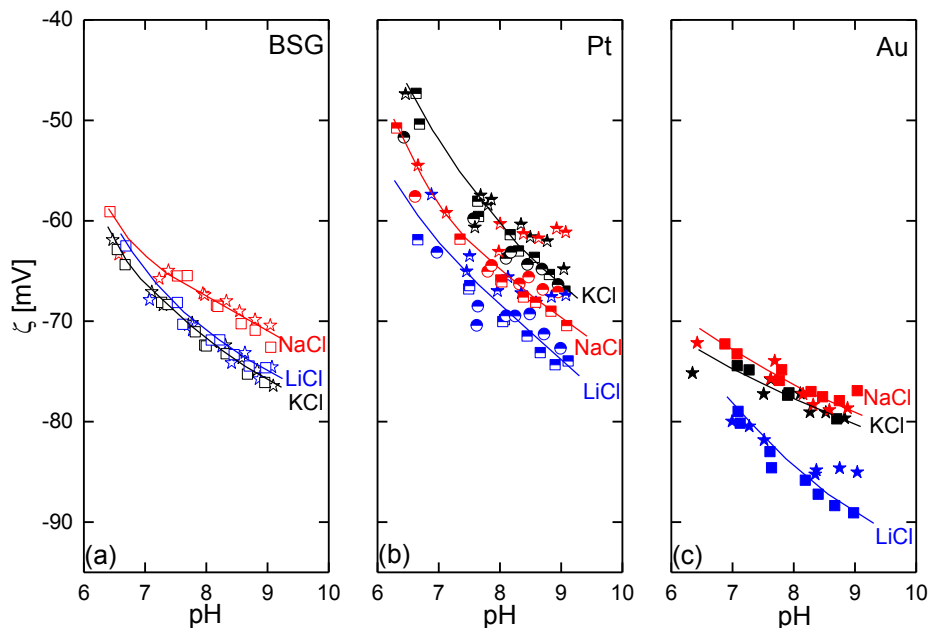


**Figure 5.6:** Time- and pH-dependent  $\zeta$  potential of BSG (a), Pt (10 nm) (b), and Au (10 nm) (c) in 10 mM XCl (X = Li, Na, or K)

The experiments are performed the same way as in the previous chapter. Directly after oxygen activation samples undergo the first basic titration (squares) and an optional consecutive basic titration (circles), followed by the last basic titration (stars) 20 h after the oxygen activation in order to analyze the stability of the activated surface. The different electrolytes are KCl (black symbols), NaCl (red symbols), and LiCl (blue symbols). The concentration of all working electrolytes is 10 mM. The main information in Figure 5.6 is:

- i. Generally, we find the “ranking” of the  $\zeta$  potential that we have already reported in the previous chapter (see Figure 5.5). Pt possesses the highest  $\zeta$  potential, followed by BSG, and, finally, Au.

- ii. With respect to the electrolyte, the ranking is more complex. For BSG, NaCl yields the highest  $\zeta$  potential, LiCl and KCl show similar results. Whereas for Au, NaCl and KCl show the highest  $\zeta$  potential. In case of Pt, KCl shows the highest  $\zeta$  potential, followed by NaCl, and, finally, LiCl.
- iii. Similar to the observation discussed in chapter 5.2.1, BSG and Au surfaces seem to be quite stable, whereas Pt shows a degradation of the activated surface for all electrolytes within the experimental time of 1 day.

The  $\zeta$  potential of BSG, Pt, and Au thin films shows different values in different chloride electrolytes XCl (X = Li, Na, or K). However, with respect to the ranking of  $\zeta$  potential in those electrolytes further research is needed.

In this chapter we demonstrate that:

- i. Independent on the electrolyte, Pt possesses the highest  $\zeta$  potential, followed by BSG, and, finally, Au.
- ii. Whereas the oxygen treatment activates the existing oxygen on the surface of BSG, it leads to a formation of a thin oxide layer on Pt and Au surfaces. This oxide layer seems to be less stable for the Pt layer than for the Au layer.
- iii. The effect of different chloride electrolytes on the pH-dependent (from pH 6 to 9)  $\zeta$  potential of BSG, Pt, and Au thin films is quite complex and not clear yet.

### 5.3 Impact of the Electrolyte Concentration on the $\zeta$ Potential

In the previous chapter we examined the impact of different electrolytes on the  $\zeta$  potential of reference sample (PP and BSG) and metallic surfaces (Pt and Au thin films). Another interesting question is, whether the electrolyte concentration plays an important role for the surface potential. This question is of great interest not only for basic research (e.g. the Debye length depends on the electrolyte concentration, and therefore the general electrical double layer model should be affected by the electrolyte concentration), but also for applications, since it could define the electrolyte concentration regime for chemical processes that rely on the surface potential.

In this chapter we will discuss the dependence of various inorganic surfaces on the electrolyte concentration. Let us start with some basic discussion of the issue in terms of the EDL model.

### 5.3.1 Basic Consideration

Figure 5.7 shows the sketch of the EDL model considering the samples with a given surface potential, the immobile layer, the mobile electrolyte layer, and the bulk electrolyte. Only the bulk electrolyte is neutral, the other components are charged.

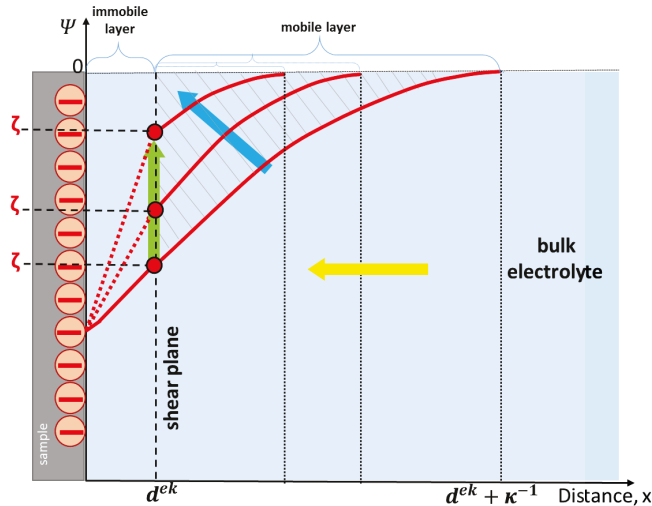


**Figure 5.7:** Sketch of the EDL model with the dashed line at distance  $d^{ek}$  and dotted line at distance  $d^{ek} + \kappa^{-1}$  defining the immobile-mobile layer interface (shear plane) and the mobile-bulk electrolyte interface, respectively. A change of electrolyte concentration leads to the change of the mobile-bulk interface (dotted lines) and the resulting potential (red lines) in the EDL.

In the streaming potential and streaming current methods, the  $\zeta$  potential is determined by the ions in the mobile layer as indicated by the shaded area in Figure 5.7. The extension of the mobile layer depends on the Debye length  $\kappa^{-1}$ . A change of the Debye length would therefore also change the potential in the EDL and, thus, the  $\zeta$  potential. A decrease of the Debye length would result in an increase of  $\zeta$  potential as long as the surface potential is not or hardly affected by this change (see Figure 5.7).

One way to modify the Debye length is to change the electrolyte concentration. Generally, the Debye length is given by:

$$\kappa^{-1} = \sqrt{\frac{\varepsilon_0 \varepsilon k_B T}{2 N_A e^2 I}} \quad , \quad (5.3)$$

where  $\varepsilon_0$  is the vacuum permittivity,  $\varepsilon$  is the dielectric constant of the electrolyte,  $k_B$  is the Boltzmann constant,  $T$  is the absolute temperature of the electrolyte,  $N_A$  is the Avogadro number,  $e$  is the elementary charge, and  $I$  is the ionic strength. For a symmetric monovalent electrolyte (e.g. KCl), the ionic strength  $I$  is equal to the electrolyte concentration  $c_B$ , i.e.  $I = c_B$ . In this way, the Debye length is:

$$\kappa^{-1} = \sqrt{\frac{\varepsilon_0 \varepsilon k_B T}{2 N_A e^2 c_B}} \quad . \quad (5.4)$$

For a given monovalent electrolyte and temperature, the Debye length only depends on the electrolyte concentration as shown in Figure 5.8.

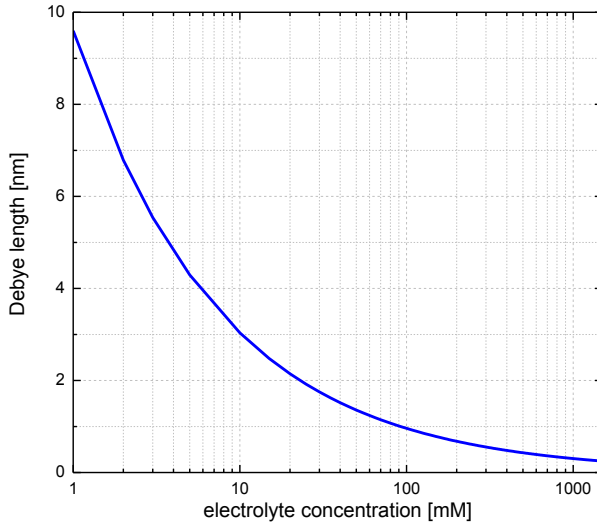


**Figure 5.8:** Dependence of the Debye length on the electrolyte concentration of a symmetric monovalent electrolyte (for  $\varepsilon = 78$  (water) and  $T = 298$  K).

### 5.3.2 Reference Measurements on Polypropylene and Borosilicate Glass

The concentration-dependent  $\zeta$  potential of polypropylene (PP) and glass (BSG) is first investigated, before we come to more complex surfaces like Pt thin films or organic molecules in the next chapter.

Since PP and BSG possess non-conductive surfaces, both the streaming potential and streaming current methods can be used to determine the  $\zeta$  potential. Since we have to use the streaming current method later for the conductive surfaces, we will use the streaming potential method in this case. For the streaming potential method, the Helmholtz-Smoluchowski equation is:

$$\zeta = \frac{dU}{dp} \frac{\eta}{\epsilon \epsilon_0} \frac{L}{AR} \quad . \quad (5.2)$$

The definition of electrical conductivity K is:

$$\frac{L}{AR} = K \quad . \quad (5.5)$$

Since the electrical conductivity K inside the measuring cell cannot be measured directly, it is commonly replaced by the bulk electrolyte conductivity  $K_B/F$ . Here F is a conductivity sensor calibration factor that has to be considered in the experiment setup. Therefore, equation 5.2 is replaced by:

$$\zeta = \frac{dU}{dp} \frac{\eta}{\epsilon \epsilon_0} \frac{K_B}{F} \quad . \quad (5.6)$$

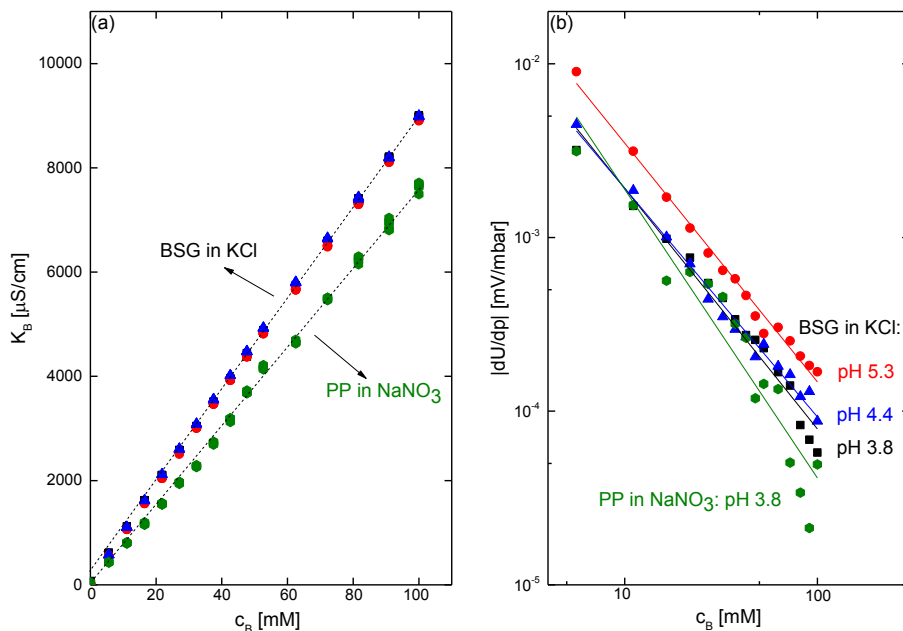


**Figure 5.9:** Dependence of electrolyte conductivity  $K_B$  (a) and the streaming potential coefficient  $dU/dp$  (b) on electrolyte concentration  $c_B$  for PP and BSG in different electrolytes.

While  $\eta$  and  $\epsilon$  are taken from a table,  $dU/dp$  and  $K_B$  are experimentally determined. Figure 5.9 shows examples for PP and BSG in KCl and  $\text{NaNO}_3$ . Obviously, in these cases  $K_B$  depends linearly on  $c_B$ , which provides the ionic strength and, thus, the conductivity of the electrolyte (see Figure 5.9a). Different dependences are observed for different electrolytes due to their different molar conductivity.  $|dU/dp|$  shows a very good linear dependence on  $c_B$  in the double logarithmic plot in all experiments (see Figure 5.9b). The linear dependence  $K_B \propto c_B$  and  $\log |dU/dp| \propto \log c_B$  given by different lines in Figure 5.9 are used for the extrapolation and prediction of the  $\zeta$  potential in Figure 5.10. The experimental data and the resulting extrapolation are shown in Figure 5.10 in form of a plot of the  $\zeta$  potential as function of the Debye length.

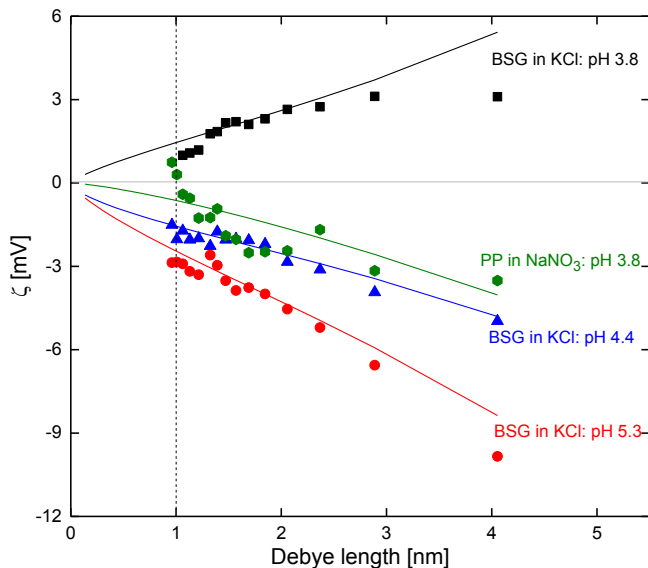


**Figure 5.10:** The experimental (dots) and calculated  $\zeta$  potential (lines) for PP and BSG as function of the Debye length.

Figure 5.10 shows a number of interesting features:

- i.  $|\zeta|$  decreases with the decrease of the Debye length, which agrees with the theoretical explanation of the EDL model (see Figure 5.7).
- ii. This decrease seems to be linear in the experiment range (down to a Debye length of  $\sim 1$  nm).
- iii. Based on this linear decrease, the extrapolation to zero Debye length would predict a zero  $\zeta$  potential (i.e.  $\zeta(\kappa^{-1} \approx 0) \approx 0$ ), which again agrees with the prediction of the EDL model.

These results confirm the EDL model. Nevertheless, they lead to two important questions:

- i. Is the observed linear dependence of the  $\zeta$  potential on the Debye length a general behavior of surface and, thus, also applicable for metallic surfaces or organic layers?
- ii. Does this linearity persist to smaller Debye length (smaller than 1 nm), i.e. electrolyte concentration higher than 100 mM?

These questions will be discussed in the next chapter.

### 5.3.3 Conductive Surfaces at Higher Electrolyte Concentration

In the last chapter, we demonstrated that the  $\zeta$  potential of nonconductive surfaces (PP and BSG) can be predicted by linear extrapolation of  $|dU/dp|$  and  $K_B$ . The validity of this extrapolation towards extremely small Debye length (i.e. high electrolyte concentration) is questionable. Moreover, deviation from the prediction might indicate that:

- i. Either the EDL model does not describe the experiments any more or
- ii. the surface potential significantly changes at high electrolyte concentration.

In this section, the  $\zeta$  potential measurements of Pt thin films are performed in different chloride electrolytes with an extended electrolyte concentration range from 5 to 1000 mM in order to test the reliability of the  $\zeta$  potential extrapolation.

#### 5.3.3.1 Extended EDL Model

Since Pt thin films have a significant surface conductance, only the streaming current method can be used to determine the  $\zeta$  potential. The corresponding Helmholtz-Smoluchowski equation is:

$$\zeta = \frac{dI}{dp} \frac{\eta}{\epsilon \epsilon_0} \frac{L}{A} \quad (5.1)$$

As before,  $\eta$ ,  $\epsilon$ ,  $L$ , and  $A$  are taken from the table or known, only  $dI/dp$  is measured. Figure 5.11 shows a typical  $dI/dp$  measurement.

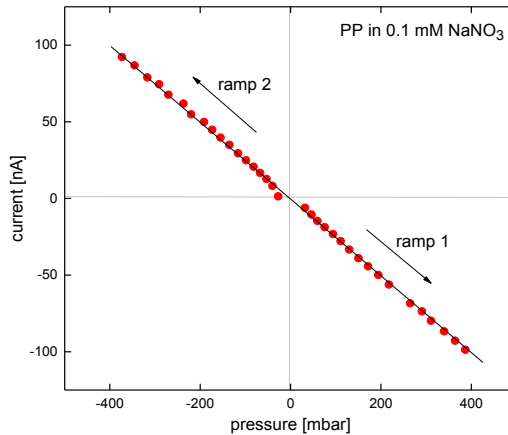


**Figure 5.11:** Typical streaming current-pressure correlation during the  $\zeta$  potential measurement at low electrolyte concentration.

Starting from zero pressure, in ramp 1 the pressure is generally increased to 400 mbar. Then in ramp 2, the flow is converted by a negative pressure from 0 to -400 mbar. The resulting streaming current shows a perfect linear dependence on pressure and there is no offset (i.e. no current at zero pressure). The slope of this linear behavior is used as streaming current coefficient  $dl/dp$  in equation 5.1 to determine the  $\zeta$  potential. In this case, the current is generated by the moving ions driven by the shear force under applied pressure and named as “shear current”. This is the ideal behavior observed for the experiments at low electrolyte concentration ( $c_B < 100$  mM) that are discussed in the previous section.

However, at high electrolyte concentration we observed nonlinear and even transient (i.e. time dependent) behavior. Three typical examples of this current-pressure correlation are shown in Figure 5.12.

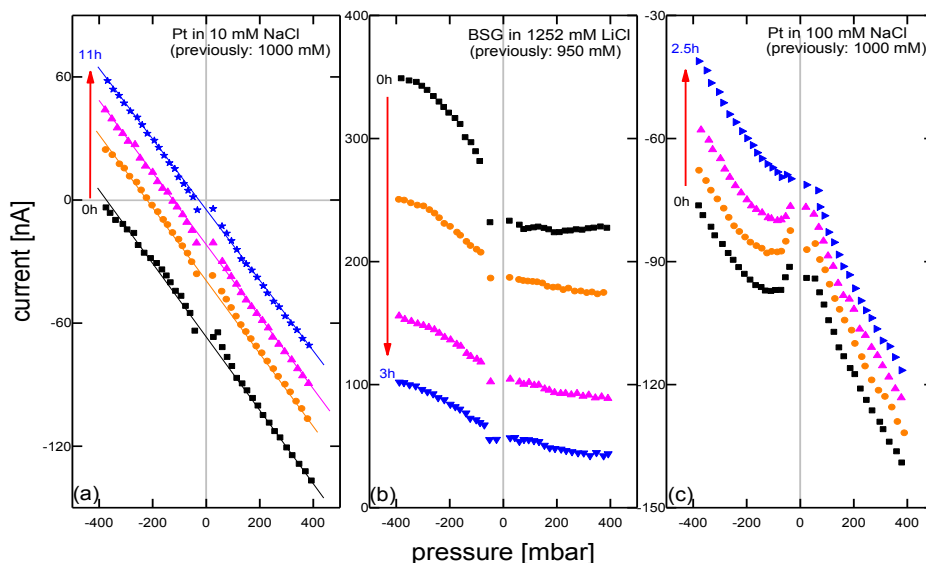


**Figure 5.12:** Examples of streaming current-pressure correlations observed when high electrolyte concentration is involved: (a) measurement after reducing the concentration from 1000 to 10 mM, (b) measurement after increasing the concentration from 950 to 1252 mM, (c) measurement after reducing the concentration from 1000 to 100 mM. All systems show transient behavior indicated by the arrows.

Since in all examples the electrolyte concentration has been changed from high to low (or vice versa), they show a transient behavior. More details are:

- i. In (a), the electrolyte concentration has been changed from 1000 to 10 mM. Due to the low concentration (10 mM), a linear current-pressure correlation is observed. Nevertheless, the offset and transient behavior indicate that there is a constant negative current, which decreases with time.
- ii. In (b), the concentration has been changed in the opposite way, i.e. from low to high. In this case we observe a positive offset, which decreases with time. Moreover, the current-pressure curves are not as linear as those in (a).
- iii. In (c), we again see the negative offset that seems to be characteristic for a change from high to low concentration like already shown in (a). However, the nonlinearity is worse than that in (a).

On the one hand, this unusual correlation causes difficulties in determining the  $\zeta$  potential. On the other hand, it shows that the process that takes place at high electrolyte concentration is more complex and might not be explained by the EDL model. Therefore, we will sketch our ideas and possible explanation for the observed current-pressure correlation in the following.

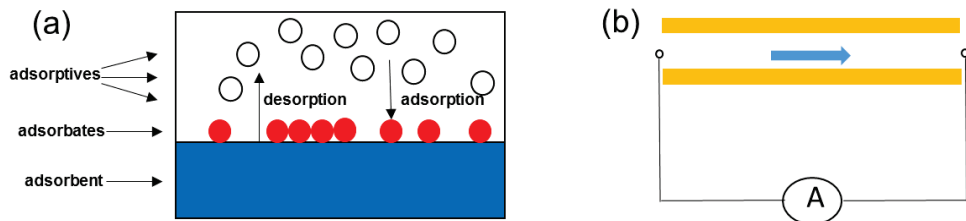


**Figure 5.13:** Ion adsorption/desorption process at the solid-liquid interface (a) and scheme of the measurement principle for the streaming current method (b).

Generally, ions adsorb and desorb at the solid-liquid interfaces (see Figure 5.13a). This adsorption and desorption leads to two main processes:

- i. It is responsible for the formation of the immobile layer of ions at the sample surface.
- ii. It can also lead to an ionic current flow, i.e. the surfaces can serve as a “source” or “drain” for ions.

Both effects can have a large impact on the resulting current-pressure curve. Moreover, they strongly depend on the electrolyte concentration and the change of the concentration. Let us explain these effects in details.

At low electrolyte concentration (typically  $c_B < 100$  mM), the immobile layer is most likely given by the classic EDL model (see Figure 5.14a). However, at high concentration, this layer might become thicker (see Figure 5.14b), and even polymerization of the hydrated ions has to be taken into account. Consequently, not only  $d^{ek}$  significantly changes at high electrolyte concentration, but also the resulting  $\zeta$  potential and the shape of the current-pressure curve are affected.

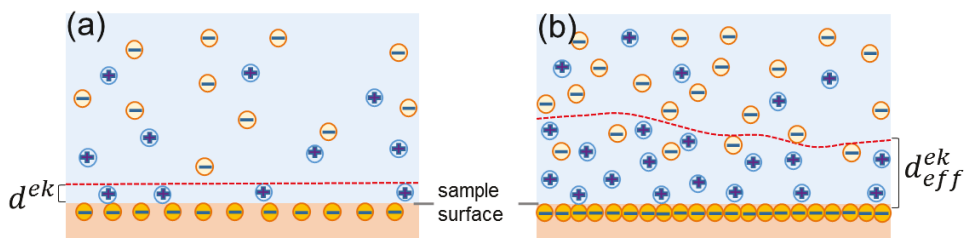


**Figure 5.14:** Schematic sketch of the sample surface states in classic EDL model (a) and extended immobile layer model (b).

The simplest situation is given for the case illustrated in Figure 5.12 (a). Here the electrolyte concentration is varied from very high (1000 mM) to quite low (10 mM). The resulting current-pressure curves are perfectly linear. However, the offset and the change of the offset indicate that, due to the change of electrolyte concentration ions are desorbed from the sample surface in the measuring cell, which leads to an additional negative current signal. With time the magnitude of the offset decreases, indicating that the thickness of the immobile layer and thus desorption rate is decreasing. Finally, the classic electrical double layer is retained and the measurement is stable without offset (see Figure 5.15).

The opposite behavior is visible in the case shown in Figure 5.12 (b). Here the electrolyte concentration is increased from 950 to 1252 mM. As a result, a large positive offset is visible, i.e. the sample surface serves as a drain for ions while the extended immobile

layer is forming. The adsorption rate reduces with time, until the final thickness of the immobile layer is reached (see Figure 5.15).

Both situations from Figure 5.12 are plotted in Figure 5.15 together with the schematic adsorption/desorption time profile expected for the change of the electrolyte concentration.

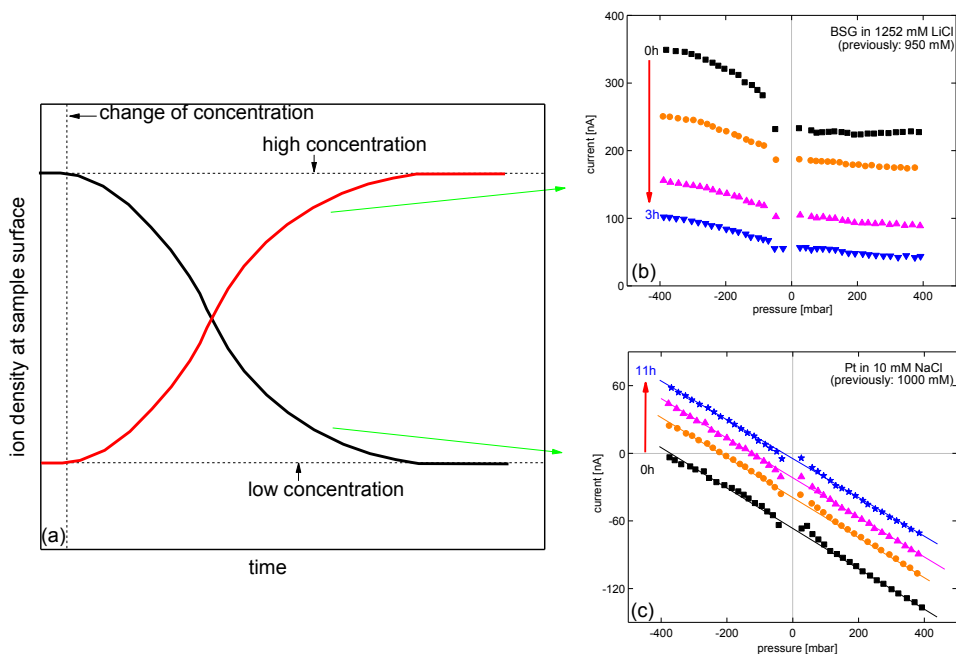


**Figure 5.15:** Schematic adsorption/desorption time profile (a) expected for the change of the electrolyte concentration, together with two corresponding examples (b, c) taken from Figure 5.12.

With the formation and removal of the extended immobile layer, we can easily explain the offset in the current-pressure curves. However, the nonlinear behavior is more complex. We believe that the explanation for this behavior is based on the flow dependence of the adsorption/desorption rate. Similar to the rate describing the deposition of thin films, the adsorption/desorption rate should depend on the number of the arriving particles. Since this number depends on the particle density and the flow, the rate should increase linearly

with the electrolyte flow up to a point where saturation sets in. Here the surface cannot adsorb any more particles. This flow dependence of the rate automatically leads to a rotation of the current-pressure correlation, which is different in direction for positive and negative flow direction. The resulting effect nicely explains the observed nonlinear current-pressure curves of Figure 5.12 (b) and (c). They are illustrated in Figure 5.16.

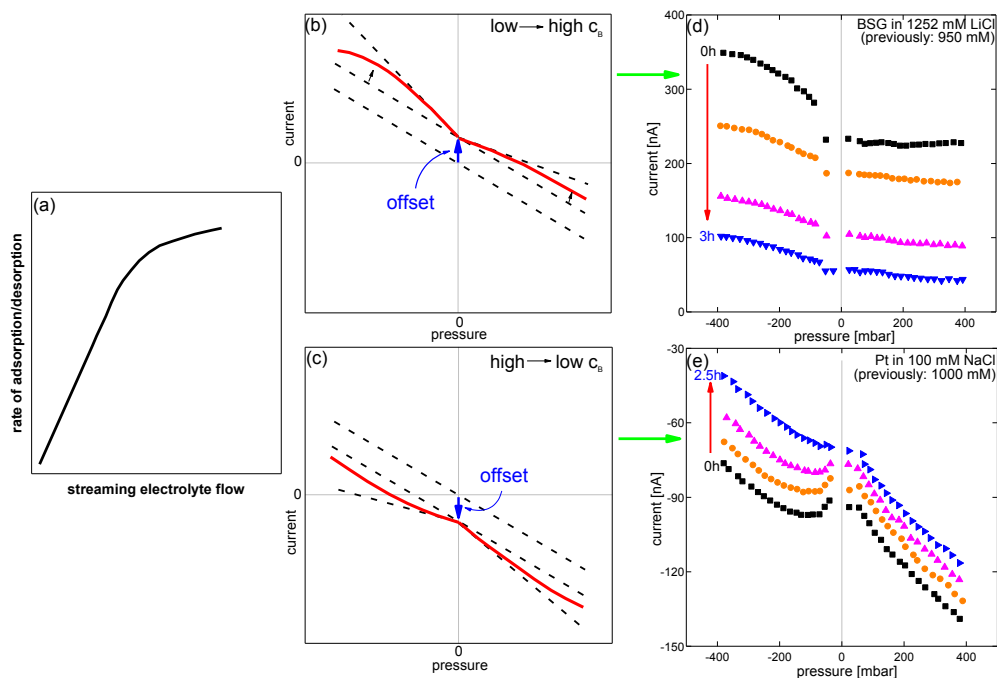


**Figure 5.16:** The flow dependence of the adsorption/desorption rate (a) together with two simulated cases (b and c), and corresponding examples (d and e) taken from Figure 5.12.

In summary, the “shear current” and the “adsorption/desorption current” comprise the total streaming current signal for the  $\zeta$  potential measurement, when high electrolyte concentration is involved. It is the “adsorption/desorption current” that causes the offset and the nonlinear current-pressure correlation at high electrolyte concentration.

The simple model including adsorption/desorption of ions and the formation of extended immobile layer at the sample surface nicely explains the experimental observed current-

pressure correlation. However, due to the nonlinear behavior it does not allow a good quantitative determination of the  $\zeta$  potential at high electrolyte concentration.

### 5.3.3.2 $\zeta$ Potential of Pt Thin Films

Since extended ion layers form at the sample surfaces at high electrolyte concentration, the measured  $\zeta$  potential shows transient behavior upon the change of the electrolyte concentration if concentration higher than 100 mM is involved. Several transient  $\zeta$  potential measurements were performed on BSG and Pt thin films. The  $\zeta$  potential is determined by using an average slope  $dI/dp$  of the 2 ramps of the current-pressure curves shown in Figure 5.17 or part of the current-pressure curves that showed reasonable linear correlation. The resulting transient behavior is shown in Figure 5.18.

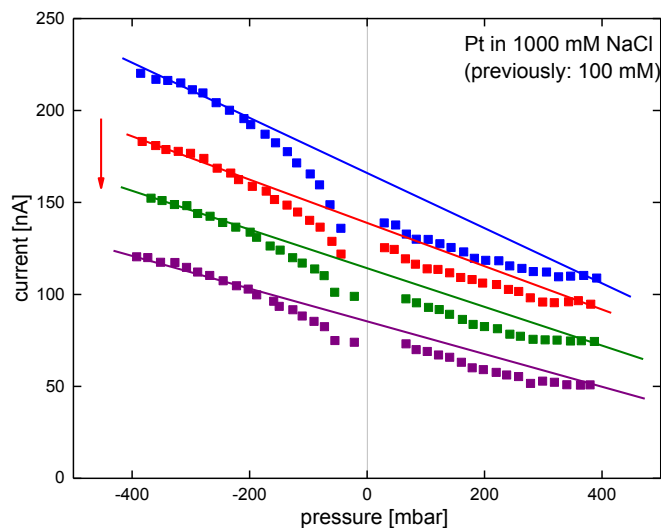


**Figure 5.17:** Current-pressure curves of transient  $\zeta$  potential measurements of 5 nm thick Pt films in 1000 mM NaCl after exposure to 100 mM NaCl.

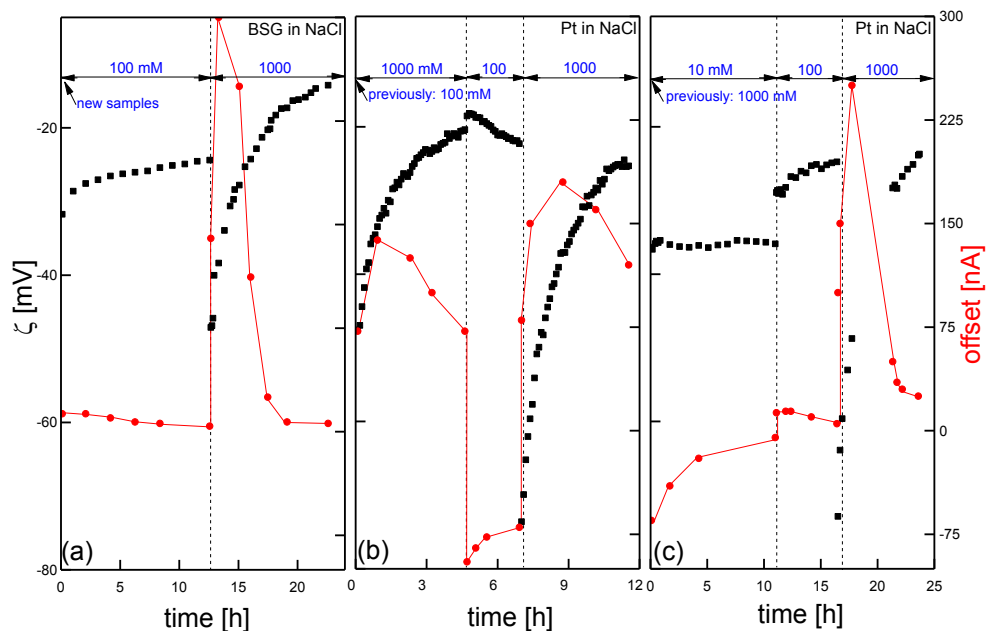


**Figure 5.18:** Transient behavior of the  $\zeta$  potential (left scale, black symbols) and offset (right scale, red symbols) for BSG (a) and Pt (b and c) in NaCl. The different concentrations (blue numbers) are given in the figures, and the dashed lines indicate the change of the electrolyte concentration.

Samples are chemically cleaned with acetone and propanol before measurements in another fresh electrolyte. There are three major points in Figure 5.18:

- i. Each electrolyte concentration change is accompanied by a jump in the offset current and the  $\zeta$  potential.
- ii. An increase of the electrolyte concentration leads to a peak in the offset current, while a decrease of the concentration leads to a minimum in the offset current (i.e. surface serves as drain or source for ions).
- iii. The direction of the jump in the  $\zeta$  potential is more complex. This will be understood after the discussion of Figure 5.20.
- iv. Finally, the offset current and the  $\zeta$  potential seem to get to saturate after the change of the electrolyte concentration.

Therefore, in order to characterize the surface potential at high electrolyte concentration, the transient behavior of the  $\zeta$  potential has to be considered. Therefore, all  $\zeta$  potential measurements were performed for 1 h for  $c_B < 100$  mM, and 3 h for  $c_B \geq 100$  mM. The measurements and the slope  $dI/dp$  used for the evaluation of the  $\zeta$  potential are shown in Figure 5.19.

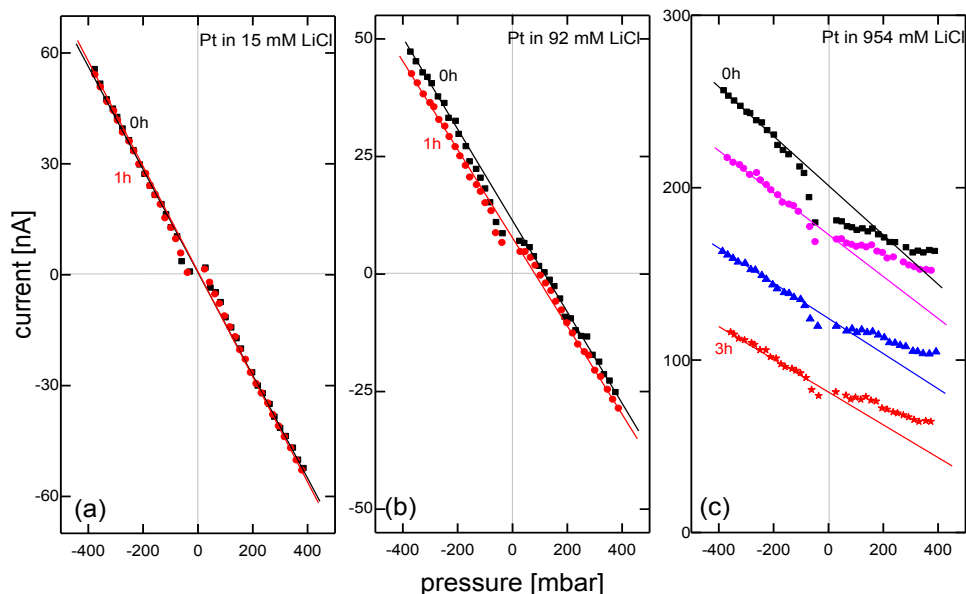


**Figure 5.19:** Experimental data and slope  $dI/dp$  of current-pressure curves recorded during concentration-dependent  $\zeta$  potential characterization of Pt films.

Based on this signal interpretation, the resulting  $\zeta$  potential is shown in Figure 5.20. Here the concentration is converted to the Debye length according to equation 5.4. The lines serve as a guide for the eye. The inset provides the same data with the Debye length in the logarithmic scale.

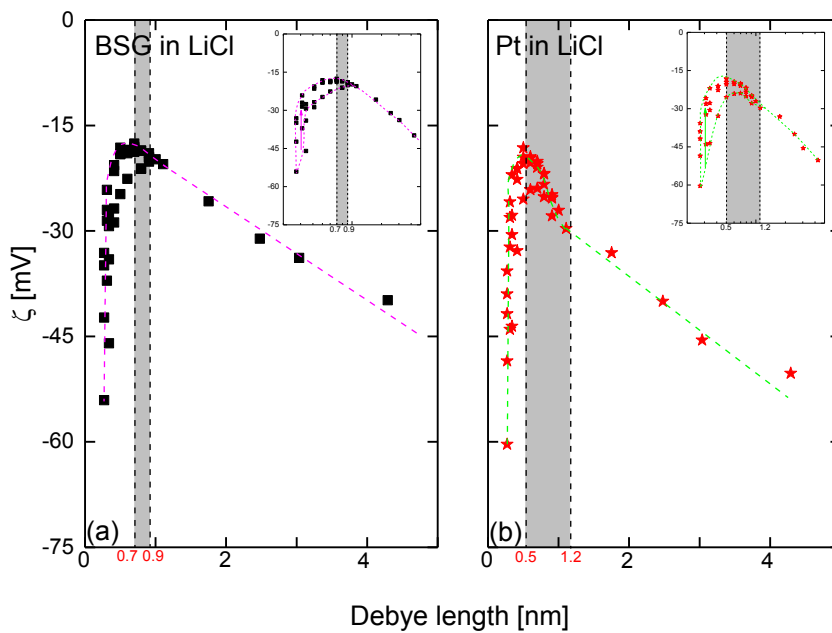


**Figure 5.20:**  $\zeta$  potential as function of the Debye length for BSG (a) and Pt (b) in LiCl. The inset shows the same data in a logarithmic scale. The shaded area marks the smallest Debye length (“critical” Debye length) for which the linear dependence of the  $\zeta$  potential can still be observed.

With the decrease of the Debye length (i.e. the increase of electrolyte concentration), the potential in the EDL and  $\zeta$  potential change in Figure 5.7. In chapter 5.3.1 a linear dependence of the  $\zeta$  potential on the Debye length (down to 1 nm) was observed for PP and BSG. Based on this linear dependence, even a zero  $\zeta$  potential is predicted due to the extrapolation to zero Debye length.

In Figure 5.20, the  $\zeta$  potential of BSG and Pt show the expected linear dependence on the Debye length for  $\kappa^{-1} > 1$  nm. However, when the Debye length gets smaller than about 1 nm (i.e. the electrolyte concentration gets higher than 100 mM), the  $\zeta$  potential does not follow this linear dependence any more. It even starts to decrease instead of increase with

decreasing Debye length. This is also the regime where the transient behavior of the  $\zeta$  potential becomes dominant (see insets of Figure 5.20).

A similar behavior of the  $\zeta$  potential as function of the Debye length is also found in electrolytes NaCl and KCl for BSG and Pt (see Figure 5.21 and 5.22).

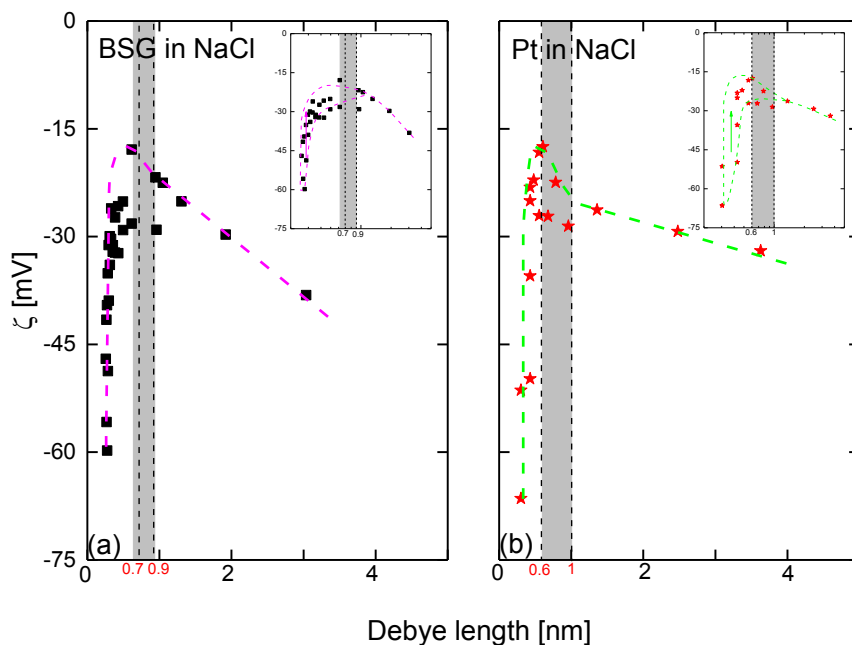


**Figure 5.21:**  $\zeta$  potential as function of the Debye length for BSG (a) and Pt (b) in NaCl. The shaded area marks the regime (“critical” Debye length), where the linear dependence of the  $\zeta$  potential on the Debye length ends.

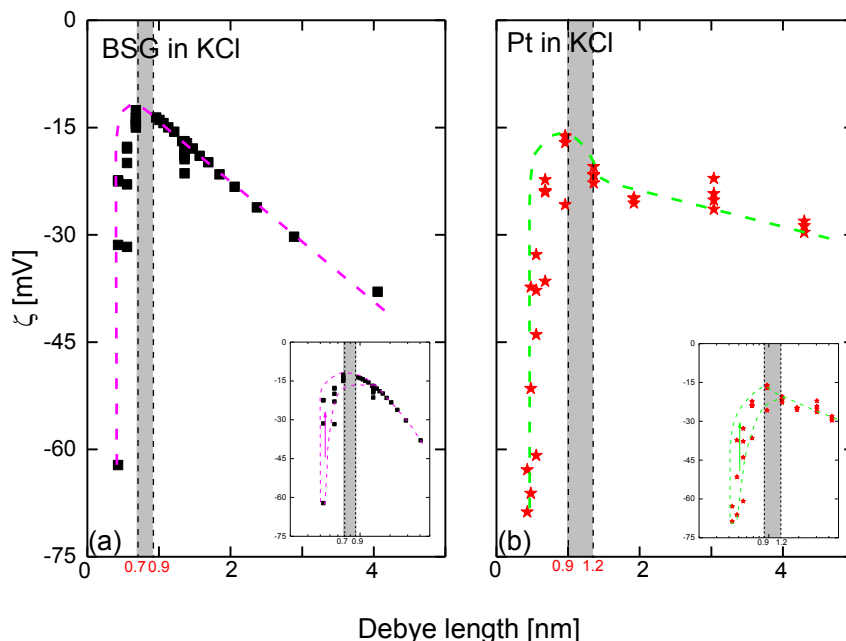


**Figure 5.22:**  $\zeta$  potential as function of the Debye length for BSG (a) and Pt (b) in KCl. The shaded area marks the “critical” Debye length.

The experimental results in different electrolytes show that the linear dependence of the  $\zeta$  potential on the Debye length is only valid down to a “critical” Debye length. Below this critical Debye length, the  $\zeta$  potential starts to decrease strongly. This observation is in contrast to the classic EDL model. There are two possible explanations for this behavior. Either the mobile layer becomes too small and therefore the approximation of the model is not valid any more, or the reaction of the electrolyte with the surface leads to a significant modification of the surface potential.

In this chapter we demonstrate that:

- i.  $|\zeta|$  of BSG and Pt decreases linearly with decreasing Debye length down to a “critical” Debye length of 0.5 – 1.2 nm, which corresponds to the electrolyte concentration of 370 – 65 mM. The critical Debye length is 0.7 – 0.9 nm for BSG and 0.5 – 1.2 nm for Pt.

- ii. At higher electrolyte concentration or smaller Debye length:
  - a. The “shear current” and the “adsorption/desorption current” comprise the total streaming current signal for the  $\zeta$  potential measurement. The latter leads to an offset current, nonlinear current-pressure curves, and a transient behavior of the  $\zeta$  potential.
  - b. The  $\zeta$  potential does not follow the linear behavior shown in the previous chapter any more. It shows a maximum at critical Debye length followed by the steep decrease of the  $\zeta$  potential. The explanation of this behavior might be that the EDL model is not applicable any more, or that the surface potential itself is strongly affected by the electrolyte.

## 5.4 $\zeta$ Potential of Organic Molecules

Due to their various functionalities, which are achieved for instance via different functional groups, self-assembling monolayers (SAMs) are often used for the modification of surface, organic electronics, or biocompatible devices. In comparison with metallic layers, self-assembled molecules possess more complex surface properties. Figure 5.23 sketches such a complex surface and it contains at least three contributions:

- i. The surface of the substrate (comparable to the classic surface that was examined in the previous sections),
- ii. the surface defined by the functional group of the molecules, and
- iii. the surfaces of the individual molecules themselves.

Due to these different contributions, the resulting  $\zeta$  potential is more complex:

$$\begin{aligned}
 I_s &= I_{\text{substrate}} + I_{\text{functional group}} + I_{\text{molecule}} \\
 &= \frac{\varepsilon\varepsilon_0 A}{\eta L} p(a_1\zeta_1 + a_2\zeta_2 + a_3\zeta_3) \quad , \quad (5.7)
 \end{aligned}$$

where the coefficients  $a_i$  ( $i = 1, 2$  or  $3$ ) characterize the different contributions. The dependence of the  $\zeta$  potential on the position  $x$  normal to the substrate might change strongly in the regime of the molecules (see Figure 5.23). By changing the Debye length, the change of the surface potential in the vicinity of the molecules might be visible.

In this section, we examine the concentration dependence of the  $\zeta$  potential of a SAM of 3-aminopropyltriethoxysilane (APTES) using the same approach shown in chapter 5.3.

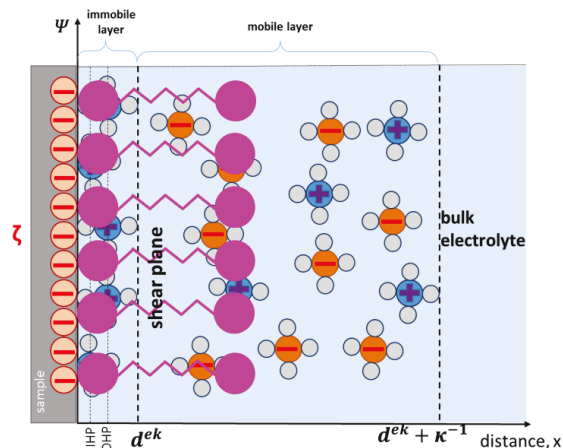


**Figure 5.23:** Sketch of the EDL model for samples with a SAM of molecules. In the vicinity of the molecules (magenta) the potential might change strongly.

APTES was deposited on chemically cleaned BSG and kept in the vacuum condition prior to the measurements (see deposition details in chapter 4.1). Before the characterization of concentration dependent  $\zeta$  potential, a standard stability test is first performed as usual. Some results of this stability test are shown in Figure 5.24.

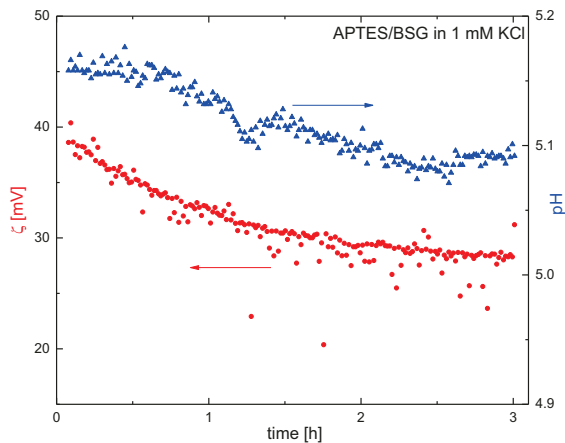


**Figure 5.24:** The stability test for a SAM of APTES on BSG in 1 mM KCl.

As always, none of the parameters are changed during the stability test. The pH value stabilizes about 5.1, while the  $\zeta$  potential decays and stabilizes after 2 h at a value of 28 mV. According to literature [15], molecules might be desorbed from the surface during the storage (that is why we stored it for 2 days in vacuum) as well as during the electrokinetic experiments. This desorption process can persist for several hours (6 h) until a stable state is reached. During our experiment, the  $\zeta$  potential does not change much after 3 h and the change is smaller compared to that in literature [15].

After the stability test, the concentration dependent  $\zeta$  potential of APTES was measured in KCl with the concentration increasing from 1 to 200 mM. Same as before, the  $\zeta$  potential measurements were performed for 1 h for  $c_B < 100$  mM and 3 h for  $c_B \geq 100$  mM.

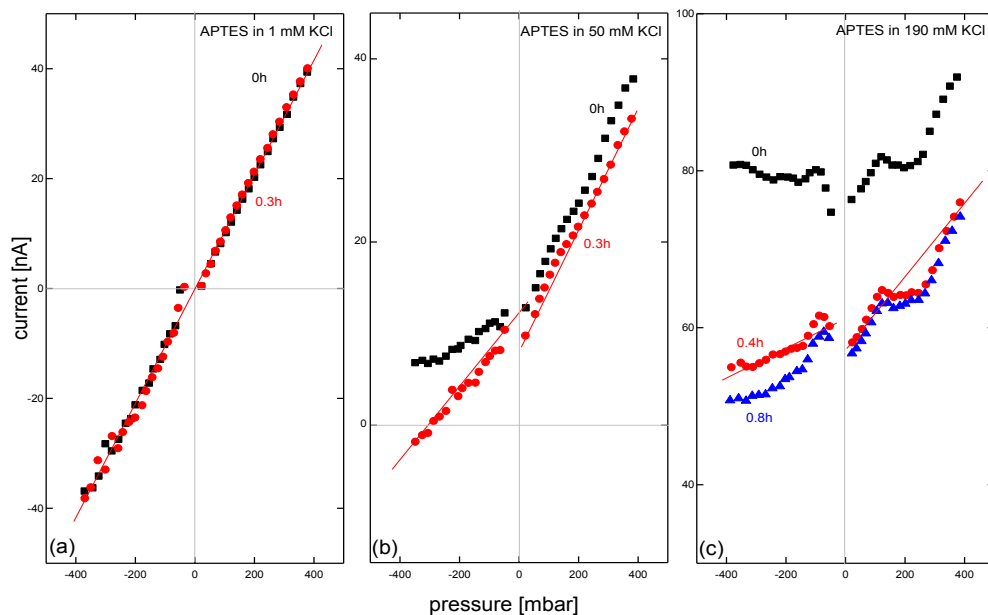


**Figure 5.25:** Determination of the slope  $dI/dp$  for the concentration dependent  $\zeta$  potential of APTES on BSG.

The slope  $dI/dp$ , necessary for the evaluation of the  $\zeta$  potential, is obtained in these experiments as indicated in Figure 5.25. We obtained a perfect linear dependence of the current on the pressure for low concentration ( $< 50$  mM), whereas at higher concentration

a current offset and a nonlinear current-pressure correlation are observed. This nonlinear current-pressure behavior is already visible for a concentration of 50 mM, which corresponds to a Debye length of 1.35 nm. This is clearly different from the behavior of Pt and BSG where we observed this nonlinearity and offset current only for concentration higher than 65 mM and 115 mM, respectively.

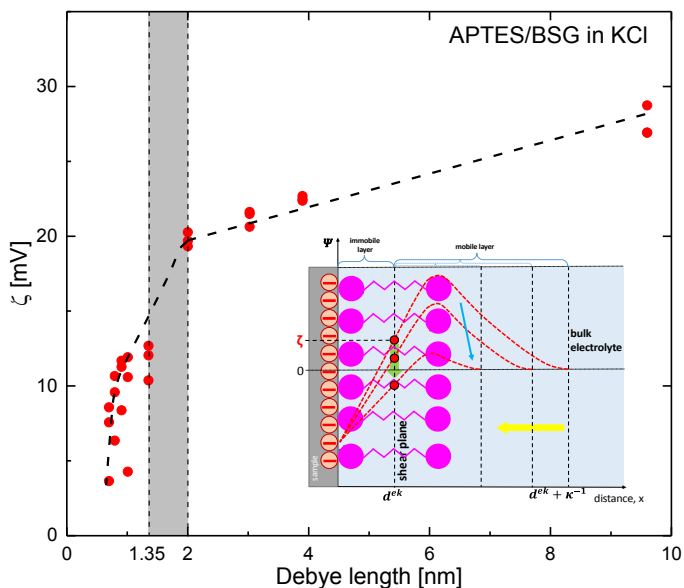


**Figure 5.26:** Concentration-dependent  $\zeta$  potential for APTES on BSG in KCl. The shaded area indicates the “critical” Debye length, and the inset sketches the change of the EDL for increasing electrolyte concentration.

Based on the signal interpretation indicated in Figure 5.25 we observe a very interesting dependence of the  $\zeta$  potential on the Debye length as shown in Figure 5.26. For low electrolyte concentration ( $c_B < 23$  mM) corresponding to a large Debye length ( $\kappa^{-1} > 2$  nm), we observe the usual linear dependence of the  $\zeta$  potential on the Debye length. However, in the regime of  $\kappa^{-1} \approx 1.35 - 2$  nm, we obtain a sudden drop in the  $\zeta$  potential. If we increase the concentration even further, we observe a strong transient behavior and a further strong decrease of the  $\zeta$  potential. The major differences with respect to the properties of the inorganic surfaces BSG and Pt are:

- i. The critical Debye length is larger, i.e. 1.35 – 2 nm in contrast to 0.5 – 1.2 nm for Pt and 0.7 – 0.9 nm for BSG.
- ii. There is an unusual drop of the  $\zeta$  potential at the critical Debye length, and
- iii. at very small Debye length the  $\zeta$  potential decreases even further in contrast to BSG and Pt, for which the surfaces show opposite behavior for low and high concentration.

All these observations can be explained by the EDL model including the molecular layer (see Figure 5.23 or inset of Figure 5.26). Due to the APTES monolayer with a thickness of 0.7 nm, the critical Debye length is enhanced in this case. For BSG it is  $\kappa_{\text{crit}}^{-1} \approx 0.8$  nm, for BSG with APTES it might be approximated by  $\kappa_{\text{crit}}^{-1} \approx 0.8 + 0.7$  nm = 1.5 nm, which fits the experimental value of 1.35 – 2 nm perfectly. By approaching the critical Debye length, the potential starts to vary strongly. This might cause the sudden change of the  $\zeta$  potential in this regime. Finally, if the Debye length is decreased even further to a length comparable to the thickness of the APTES monolayer (0.7 nm), the  $\zeta$  potential might become even negative due to the negative surface potential of BSG. Therefore, we observe a second very strong decrease of the  $\zeta$  potential at very small Debye length.

Although only a few experiments were performed on APTES, it already demonstrates that a more complex and interesting situation shows up for these organic systems. In order to characterize the surface properties of APTES or other organic molecules, more investigation needs to be done.

In this chapter we showed the concentration dependent measurements of the  $\zeta$  potential of SAMs (APTES on BSG).

- i. The  $\zeta$  potential decreases linearly with decreasing Debye length down to a critical Debye length in the range of 1.35 – 2 nm, which is larger than the critical Debye length observed for Pt ( $\kappa_{\text{crit}}^{-1} \approx 0.5$  – 1.2 nm) and BSG ( $\kappa_{\text{crit}}^{-1} \approx 0.7$  – 0.9 nm).
- ii. Below the critical Debye length, a sudden drop of the  $\zeta$  potential is observed, followed by a further strong decrease of the  $\zeta$  potential once the Debye length becomes comparable to the thickness of APTES monolayer (0.7 nm).
- iii. All these observations can be explained in terms of the EDL model taking the additional contributions of the molecular layer into account.

## 6 Conclusions

The surface potential represents one of the key properties of the solid-liquid interface, and is important for many fields like the growth of inorganic thin films or organic molecular layers as well as biological experiments. In the classic electrical double layer (EDL) model, which is typically used to describe the solid-liquid interface, the  $\zeta$  potential is used to characterize the surface potential.

In this thesis, the  $\zeta$  potential of different surfaces (polypropylene (PP), borosilicate glass (BSG), Pt thin films, Au thin films, and SAM of APTES on BSG) and its modification via oxygen activation and electrolyte concentration variation are discussed. The experiments were performed with a modified “SurPASS Electrokinetic Analyzer” using the streaming potential and streaming current methods. Starting with the measurements on PP and BSG that show the reliability of the setup and serve as reference measurements, we demonstrate:

- i. Independent on the electrolyte, Pt films possess the highest  $\zeta$  potential, followed by BSG, and, finally, Au films. The effect of different chloride electrolytes XCl (X = Li, Na, or K) on the  $\zeta$  potential of these three systems (BSG, Pt, and Au) turned out to be more complex.
- ii. The  $\zeta$  potential is sensitive to surface treatments. Oxygen activation via ozone seems to form a thin oxide layer on the Pt and Au surfaces. The oxide layer seems to be less stable for the Pt layer than for the Au layer. In case of the BSG, the oxygen activation leads to a stable activation of the oxide surface, which is visible in a stable reduction of the  $\zeta$  potential.
- iii. Finally, the most interesting results were obtained for concentration dependent  $\zeta$  potential measurements performed on BSG, Pt films and an organic molecular layer (i.e. SAM of APTES on BSG). By varying the electrolyte concentration, the Debye length (i.e. the thickness of the mobile layer of the EDL) is modified. In all three cases, we observe a linear decrease of  $|\zeta|$  with decreasing Debye length. At the critical Debye length this behavior abruptly changes. The  $\zeta$  potential shows a strong kink and a transient behavior sets in. We explain this change by a new model, which comprises the total streaming current by the standard “shear current”

and an additional “adsorption/desorption current”. The latter leads to an offset current, a nonlinearity in the current-pressure curves, and a transient behavior of the  $\zeta$  potential. Also the kink in the  $\zeta$  potential behavior at the critical Debye length can be explained by this model. However, it is not clear whether the kink is only an indication that the EDL model does not work any more (e.g. the immobile layer becomes thicker at high electrolyte concentration), or whether it is an indication that the surface potential itself differs strongly from the potential expected by the extrapolation of the  $\zeta$  potential measured at low electrolyte concentration. In any case, the critical Debye length is different for different systems. It is smaller for BSG (0.7 – 0.9 nm), followed by Pt (0.5 – 1.2 nm), and finally APTES (1.35 – 2 nm). Also the behavior of the  $\zeta$  potential for the Debye length smaller than the critical Debye length is different for the simple BSG and Pt compared to the complex surface of APTES on BSG. Both observations support the second assumption, i.e. the surface potential itself affects the  $\zeta$  potential for the Debye length smaller than the critical Debye length.

The systematic comparison of different solid-liquid interfaces using on the one hand oxide, metallic and organic surfaces, and on the other hand different electrolytes XCl (X = Li, Na, or K) with different concentration ranging from 5 to 1200 mM provides an interesting and unique insight into the complexity of surface properties and options to modify them for various applications.

## 7 References

- [1] A. Sze, D. Erickson, L. Ren, and D. Li, "Zeta-potential measurement using the Smoluchowski equation and the slope of the current–time relationship in electroosmotic flow," *Colloid and Interface Science*, vol. 261, pp. 402–410, 2003.
- [2] C. Kaulen, M. Homberger, S. Bourone, N. Babajani, S. Karhäuser, A. Besmehn, and U. Simon, "Differential adsorption of gold nanoparticles to gold/palladium and platinum surfaces," *Langmuir*, vol. 30, pp. 574–583, 2014.
- [3] S. Roessler, R. Zimmermann, D. Scharnweber, C. Werner, and H. Worch, "Characterization of oxide layers on Ti6Al4V and titanium by streaming potential and streaming current measurements," *Colloid and Interface Science*, vol. 26, pp. 387–395, 2002.
- [4] A. Shukla and H. Rehage, "Zeta potentials and Debye screening lengths of aqueous, viscoelastic surfactant solutions (cetyltrimethylammonium bromide/sodium salicylate system)," *Langmuir*, vol. 24, pp. 8507–8513, 2008.
- [5] "Assessing the zeta potential at high salinity," *Anton Paar Application Report*, Jun. 2015.
- [6] D. Erickson, D. Li, and C. Werner, "An improved method of determining the  $\zeta$ -potential and surface conductance," *Colloid and Interface Science*, vol. 232, pp. 186–197, 2000.
- [7] S. Salgin, U. Sagin, and N. Soyer, "Streaming potential measurements of polyethersulfone ultrafiltration membranes to determine salt effects on membrane zeta potential," *Int. J. Electrochem. Sci.*, vol. 8, pp. 4073–4084, 2013.
- [8] E. E. Saka and C. Güler, "The effects of electrolyte concentration, ion species and pH on the zeta potential and electrokinetic charge density of montmorillonite," *Clay Minerals*, vol. 41, pp. 853–861, 2006.
- [9] C. Werner, R. Zimmermann, and T. Kratzmüller, "Streaming potential and streaming current measurements at planar solid/liquid interfaces for simultaneous determination of zeta potential and surface conductivity," *Colloids and Surfaces A*, vol. 192, pp. 205–213, 2001.
- [10] P. Fievet, M. Sbai, A. Szymczyk, and A. Vidonne, "Determining the  $\zeta$ -potential of plane membranes from tangential streaming potential measurements: effect of the

- membrane body conductance,” *Journal of Membrane Science*, vol. 226, pp. 227–236, 2003.
- [11] A. M. Gallardo-Moreno, V. Vadillo-Rodriguez, J. Perera-Nunez, J. M. Bruqueab, and M. L. Gonzalez-Martin, “The zeta potential of extended dielectrics and conductors in terms of streaming potential and streaming current measurements,” *Phys. Chem. Chem. Phys.*, vol. 14, pp. 9758–9767, 2012.
- [12] H. Xie, T. Saito, and M. A. Hickner, “Zeta potential of ion-conductive membranes by streaming current measurements,” *Langmuir*, vol. 27, pp. 4721–4727, 2011.
- [13] A. Yaroshchuk and T. Luxbacher, “Interpretation of electrokinetic measurements with porous films: role of electric conductance and streaming current within porous structure,” *Langmuir*, vol. 26, no.13, pp. 10882–10889, 2010.
- [14] “Influence of porous structure on electrokinetic properties of polymer membranes,” *Anton Paar Application Report*.
- [15] K. Greben, “Modification and characterization of potential bioelectronic interfaces”, 2015.
- [16] A. Markov, K. Greben, D. Mayer, A. Offenhäusser, and R. Wördenweber, “In situ analysis of the growth and dielectric properties of organic self-assembled monolayers: A way to tailor organic layers for electronic applications,” *ACS Appl. Mater. Interfaces*, vol. 8, no. 25, pp. 16451–16456, 2016.
- [17] T. Luxbacher, *The ZETA Guide: Principles of the streaming potential technique*, 1st ed. Graz: Anton Paar GmbH, pp. 137, 2014.
- [18] R. Zimmermann, U. Freudenberg, R. Schweiß, D. Küttner, and C. Werner, “Hydroxide and hydronium ion adsorption — A survey,” *Curr. Opin. Colloid Interface Sci.*, vol. 15, no. 3, pp. 196–202, Jun. 2010.
- [19] D. Stawski and C. Bellmann, “Electrokinetic properties of polypropylene textile fabrics containing deposited layers of polyelectrolytes,” *Colloids Surfaces A Physicochem. Eng. Asp.*, vol. 345, no. 1–3, pp. 191–194, Aug. 2009.
- [20] B. Kořikova, A. Revajova, and V. Demianova, “The effect of adding lignin on modification of surface properties of polypropylene,” *Eur. Polym. J.*, vol. 31, no. 10, pp. 953–956, 1995.

- [21] Z. Kolská, N. S. Kasálková, J. Siegel, and V. Švorčík, "Electrokinetic potential for characterization of nanostructured solid flat surfaces," *Journal of Nano Research*, vol. 25, pp. 31–39, 2013.
- [22] I. Aranberri-Askargorta, T. Lampke, and A. Bismarck, "Wetting behavior of flax fibers as reinforcement for polypropylene," *J. Colloid Interface Sci.*, vol. 263, pp. 580–589, 2003.
- [23] F. Borghi, V. Vyas, A. Podesta, and P. Molani, "Nanocscale roughness and morphology affect the isoelectric point of titania surfaces," *PLOS, journal.pone.0068655*, 2013.
- [24] M. Kosmulski, "A literature survey of the differences between the reported isoelectric points and their discussion," *Colloids Surfaces A Physicochem. Eng. Asp.*, vol. 222, no. 1–3, pp. 113–118, Jul. 2003.
- [25] M. Kosmulski, "The pH-dependent surface charging and points of zero charge: V. Update.," *J. Colloid Interface Sci.*, vol. 353, no. 1, pp. 1–15, Jan. 2011.
- [26] J. Lyklema, "Overcharging, charge reversal: chemistry or physics?" *Colloids Surfaces A Physicochem. Eng. Asp.*, vol. 291, no. 1–3, pp. 3–12, Dec. 2006.
- [27] Z. Li, P. Beck, D. A. Ohlberg, D. R. Stewart, and R. S. Williams, "Surface properties of platinum thin films as a function of plasma treatment conditions" *Surface Science*, vol. 529, pp. 410–418, 2003.
- [28] D. Y. Zemlyanov, B. R. Fingland, and A. Wei etc., "Plasma cleaning applications for surface science and model catalyst samples", *Microsc Microanal*, vol. 15 (Suppl. 2), pp. 816–817, 2009.

## **Acknowledgement**

This master thesis is done in Peter Grünberg Institute / Institute of Complex Systems (PGI-8/ICS-8) in Forschungszentrum Jülich, supervised by Prof. Dr. Roger Wördenweber. It is also supervised by the Department of Corrosion and Corrosion Protection in RWTH Aachen.

First of all, I am very grateful to Prof. Dr. Roger Wördenweber for always guiding me during the work, for teaching me how to handle scientific processes, how to work efficiently, and how to cooperate in the multicultural environment. I show a great appreciation to my colleagues Alexandr Markov, Rolf Kutzner, and Yang Dai for all assistance and support in my work. A great gratitude is certainly given to all of my colleagues for being very kind to me and providing a pleasant work atmosphere. I want to thank Corinna Kaulen from IAC of RWTH Aachen for the support and help. I also want to thank Prof. Dr. Andreas Offenhäusser for giving me the chance to work in this institute. I would like to express my gratitude to Prof. Dr. Daniela Zander and Ms. Veronika Chaineux for their support and helpful advice.

Band / Volume 123

**Group IV Epitaxy for Advanced Nano- and Optoelectronic Applications**

S. Wirths (2016), vi, 116, XXX pp

ISBN: 978-3-95806-132-3

Band / Volume 124

**Strained Silicon-Germanium/Silicon Heterostructure Tunnel FETs for Low Power Applications**

S. Blaeser (2016), iv, 91, xvii pp

ISBN: 978-3-95806-135-4

Band / Volume 125

**Nanocavity Arrays for Extracellular Recording and Stimulation of Electroactive Cell Systems**

A. Czeschik (2016), x, 162 pp

ISBN: 978-3-95806-144-6

Band / Volume 126

**Band Structure Engineering in 3D Topological Insulators Investigated by Angle-Resolved Photoemission Spectroscopy**

M. Eschbach (2016), VIII, 153 pp

ISBN: 978-3-95806-149-1

Band / Volume 127

**Dynamics in colloid and protein systems: Hydrodynamically structured particles, and dispersions with competing attractive and repulsive interactions**

J. Riest (2016), ix, 226 pp

ISBN: 978-3-95806-153-8

Band / Volume 128

**Self-purifying  $\text{La}_{2/3}\text{Sr}_{1/3}\text{MnO}_3$  epitaxial films: Observation of surface precipitation of  $\text{Mn}_3\text{O}_4$  particles for excess Mn ratios**

A. Steffen (2016), 154 pp

ISBN: 978-3-95806-162-0

Band / Volume 129

**Strain and electric field mediated manipulation of magnetism in  $\text{La}_{(1-x)}\text{Sr}_x\text{MnO}_3/\text{BaTiO}_3$  heterostructures**

M. Schmitz (2016), VI, 141 pp

ISBN: 978-3-95806-164-4

Band / Volume 130

**High-Throughput Live-Cell Imaging for Investigations of Cellular Heterogeneity in *Corynebacterium glutamicum***

S. Helfrich (2016), xvi, 217 pp

ISBN: 978-3-95806-167-5

Band / Volume 131

**Laser-Induced Ultrafast Electron- and Spin-Dynamics in the Electronic Band Structure of Co(001)**

M. A. Plötzing (2016), ii, 109, XXXIV pp

ISBN: 978-3-95806-168-2

Band / Volume 132

**Robot-Assisted Phenotyping of Genome-Reduced *Corynebacterium glutamicum* Strain Libraries to Draft a Chassis Organism**

S. Unthan (2016), 122 pp

ISBN: 978-3-95806-169-9

Band / Volume 133

**Characterization of amino acid ammonia lyases & aminomutases for the production of chiral  $\alpha$ - and  $\beta$ -amino acids**

A. Dreßen (2016), ix, 112 pp

ISBN: 978-3-95806-176-7

Band/Volume 134

**7th Georgian-German School and Workshop in Basic Science**

Kacharava, A. (Ed.) erscheint nur als CD (2016)

ISBN 978-3-95806-179-8

Band / Volume 135

**Crystal growth and scattering studies on two ferrites**

S. Adiga (2016), iv, 150 pp

ISBN: 978-3-95806-183-5

Band / Volume 136

**Manipulating the Structural and Electronic Properties of Epitaxial  $\text{NaNbO}_3$  Films via Strain and Stoichiometry**

B. Cai (2016), VI, 114 pp

ISBN: 978-3-95806-185-9

Band / Volume 137

**Surface Potential of Metallic Surfaces and Self-Assembling Organic Monolayers in Various Electrolytes**

J. Wang (2016), ii, 58 pp

ISBN: 978-3-95806-188-0

Weitere **Schriften des Verlags im Forschungszentrum Jülich** unter

<http://www.zb1.fz-juelich.de/verlagextern1/index.asp>



**Schlüsseltechnologien /  
Key Technologies  
Band / Volume 137  
ISBN 978-3-95806-188-0**

